# Numerical study of particle suspensions in Newtonian and non-Newtonian fluids

by

Dhiya Abdulhussain Alghalibi

December 2019
Technical Reports
Royal Institute of Technology
Department of Mechanics
SE-100 44 Stockholm, Sweden

Akademisk avhandling som med tillstånd av Kungliga Tekniska Högskolan i Stockholm framlägges till offentlig granskning för avläggande av teknologie doctorsexamen Fredag den 6 December 2019 kl 10:15 i Ångdomen (Rumsnr: 5209), Osquars backe 31, KTHB, våningsplan 2, KTH Campus, Stockholm.

TRITA-MEK 2019;55
ISSN 0384-467X
ISRN KTH/MEK/TR-19/55-SE
ISBN 978-91-7873-385-9

*Cover:* Instantaneous snapshot of the particle arrangement for a laminar shear thinning Couette flow, $\dot{\gamma} = 0.1$, $Re_p = 0.5$ and $\Phi = 40\%$. Particles are colored according to their velocity in the streamwise direction, where the red and blue colors denote the negative and positive directions, respectively. Particle diameters are shown at their actual size.



Universitetsservice US–AB, Stockholm 2019

*Dedicated to my lovely family ...*

# Numerical study of particle suspensions in Newtonian and non-Newtonian fluids

**Dhiya Abdulhussain Alghalibi**
Linné FLOW Centre, KTH Mechanics, Royal Institute of Technology
SE-100 44 Stockholm, Sweden.

## Abstract

Solid or deformable particles suspended in a viscous fluid are of scientific and technological interest in a broad range of applications. Pyroclastic flows from volcanoes, sedimentation flows in river bed, food industries, oil-well drilling, as well as blood flow in the human body and the motion of suspended micro-organisms in water (like plankton) are among the possible examples. Often, in these particulate flows, the carrier fluid might exhibit an inelastic or a visco-elastic non-Newtonian behavior. Understanding the behavior of these suspensions is a very difficult task. Indeed, the complexities and challenges of multiphase flows are mainly due to the large number of governing parameters such as the physical properties of the particles (e.g., shape, size, stiffness, density difference with suspended fluid, solid volume fraction), the large set of interactions among particles and the properties of the carrier fluid (Newtonian or non-Newtonian); variations of each of these parameters may provide substantial quantitative and qualitative changes in the behavior of the suspension and affect the overall dynamics in several and sometimes surprising ways. The aim of this work is therefore to provide a deeper understanding of the behavior of particle suspensions in laminar Newtonian and non-Newtonian (inelastic and/or visco-elastic) fluid flows for a wide range of different parameters. To this purpose, particle-resolved direct numerical simulations of spherical particles are performed, using an efficient and accurate numerical tool. The code is based on the Immersed Boundary Method (IBM) for the fluid-solid interactions with lubrication, friction and collision models for the close range particle-particle (particle-wall) interactions. Both inelastic (Carreau and power-law), and visco-elastic models (Oldroyd-B and Giesekus) are employed to investigate separately the shear-thinning, shear-thickening, viscoelastic and combined shear-thinning visco-elastic features of the most commonly encountered non-Newtonian fluids. Moreover, a fully Eulerian numerical algorithm based on the one-continuum formulation is used to examine the case of an hyper-elastic neo-Hookean deformable particle suspended in a Newtonian flows.

Firstly, we have investigated suspensions of solid spheres in Newtonian, shear thinning and shear thickening fluids in the simple shear flow created by two walls moving in opposite directions, considering various solid volume fractions and particle Reynolds numbers, thus including inertial effects. The results show that that the non-dimensional relative viscosity of of the suspension and the mean value of the local shear-rate can be well predicted by homogenization theory, more accurately for lower particle concentrations. Moreover, we show that in

the presence of inertia, the effective viscosity of these suspensions deviates from that of Stokesian suspensions.

We also examine the role of fluid elasticity, shear-thinning and combined shear-thinning visco-elastic effects on the simple linear Couette shear flow of neutrally-buoyant rigid spherical particles. It is found that the effective viscosity grows monotonically with the solid volume fraction and that all the Non-Newtonian cases exhibit a lower effective viscosity than the Newtonian ones; in addition, we show that elastic effects dominate at low elasticity whereas shear thinning is predominant at high applied shear rates. These variations in the effective viscosity are mainly due to changes in the particle-induced shear stress component.

We then study the settling of spherical particles in quiescent wall-bounded Newtonian and shear-thinning fluids at three different solid volume fractions. We find that the mean settling velocities decrease with the particle concentration as a consequence of the hindering effect and that the mean settling speed is always larger in the shear thinning fluid than in the Newtonian one, due to the reduction of the local fluid viscosity around the particles which leads to a lower drag force acting on the particles.

Finally, the inertial migration of hyper-elastic deformable particle in laminar pipe flows is also investigated. We consider different flow rates and various levels of particle elasticity. We observe that the particle deforms and experiences a lateral movement while traveling downstream through the pipe, always finding a stable position at the pipe centerline.

**Key words:** inertial suspensions, rheology, non-Newtonian fluids, visco-elastic, sedimentation, deformable particle, hyper-elastic.

# Numerisk studie av partikelsuspensioner i Newtonska och icke-Newtonska vätskor

**Dhiya Abdulhussain Alghalibi**
Linné FLOW Centre, KTH Mekanik, Kungliga Tekniska Högskolan
SE-100 44 Stockholm, Sverige.

## Sammanfattning

Suspensioner av solida eller deformerbara partiklar i viskösa vätskor är av vetenskapligt och teknologiskt intresse för ett stort spann av applikationer. Några typiska exempel inkluderar pyroklastiska flöden från vulkaner, sedimenterande flöden i flodbäddar, livsmedelsindustrin, oljebrunnsborrning, blodflödet i människokroppen samt rörelsen hos mikroorganismer (till exempel plankton) i havet. I dessa partikelflöden kan den bärande vätskan ha ett icke-elastiskt eller viskoelastiskt icke-Newtonskt beteende. Att förstå beteendet hos dessa suspensioner är en mycket svår uppgift. Komplexiteten hos, och utmaningen med, multifasflöden beror till största delen på det stora antal styrande parametrar. Dessa inkluderar de fysikaliska partikelegenskaperna (till exempel form, storlek, styvhet, densitetsskillnad mot det bärande mediet samt volymfraktion), den stora mängden interaktioner mellan partiklarna samt egenskaperna hos den bärande fluiden (Newtonsk eller icke-Newtonsk). Variationer i vardera av dessa parametrar kan leda till stora kvantitativa och kvalitativa förändringar i suspensionens beteende och kan påverka den övergripande dynamiken på många, ibland överraskande, sätt. Målet med denna avhandling är därför att ge en djupare förståelse av partikelsuspensioner i laminära, Newtonska och icke-Newtonska (icke-elastiska och/eller visko-elasiska), flöden för ett stort spann av parametrar. För detta används ett effektivt och precist simuleringsverktyg som tillåter partikelupplösta, numeriska simuleringar av sfäriska partiklar. Koden är baserad på Immersed boundary-metodiken (IBM) för fluid-strukturinteraktion med lubrikations-, friktions- och kollisionsmodeller för partikel-partikel- och partikel-vägginteraktioner. Både icke-elastiska (Carreau och power-law) och viskoelastiska (Oldroyd-B och Giesekus) modeller betraktades för att, i isolering, undersöka effekterna av skjuvförtunnande, skjuvförtjockande, viskoelasticitet samt kombinationen av skjuvförtunning och viskoelastik, vilka vanligen förekommer hos icke-Newtonska fluider. Därutöver användes en Eulerisk numerisk algoritm baserad på en en-kontinuumformulering för att undersöka fallet med en hyperelastisk, neo-Hookisk och deformerbar partikel i en Newtonsk vätska.

Till att börja med undersöks suspensioner av solida sfärer i Netwonska, skjuvförtunnande samt skjuvförtjockande fluider i ett skjuvflöde genererat mellan två väggar som rör sig i motsatt riktning. Varierande volymfraktioner (av partiklar) och partikel-Reynoldstal (dvs inkluderande av fluidtröghet) betraktas. Resultaten visar att den dimensionslösa relativa viskositeten hos suspensionen

och medelvärdet av den lokala skjuvhastigheten kan väl förutsägas av homogeniseringsteori, speciellt tillförlitligt vid låga partikelkoncentrationer. Därutöver visas att den effektiva viskositeten hos dessa suspensioner avviker från suspensioner i Stokesflöde när flödeströghet inkluderas.

Därutöver undersöktes rollen hos elasticitet, skjuvförtunnande samt kombinerad skjuvförtunnande och viskoelasticitet i det bärande mediet på ett linjärt Couetteflöde med densitetsmatchade, rigida och sfäriska partiklar. Den effektiva viskositeten växer monotont med partikelvolymfraktionen och alla icke-Newtonska fall uppvisar en lägre effektiv viskositet än de motsvarande Newtonska fallen. Det visas även att elastiska effekter dominerar vid låg elasticitet medan skjuvförtunnande effekter dominerar vid höga skjuvhastigheter. Dessa variationer i effektiv viskositet beror främst på förändringar i den partikelinducerade komponenten av skjuvspänningen.

Efter detta studeras sedimentering av sfäriska partiklar i ett stillastående flöde mellan två väggar. Både Newtonska och skjuvförtunnande vätskor betraktas vid tre olika partikelvolymfraktioner. Det visas att medelvärdet av sedimenteringshastigheten minskar med partikelkoncentration på grund av den hindrande effekten av omgivande partiklar. Därutöver är medelsedimentationshastigheten alltid större i en skjuvförtunnande än en Newtonsk vätska på grund av reduktionen i lokal fluidviskositet runt partiklarna, vilket leder till en lägre motståndskraft.

Slutligen undersöks även tröghetsinducerad migration av hyperelastiska och deformerbara partiklar i ett laminärt rörflöde. Olika flöden och nivåer av elasticitet hos partikeln betraktas. Partikeldeformation och lateral rörelse observeras för partiklarna när de rör sig nedströms längs röret, vilket leder till att partiklarna alltid finner en stabil position vid rörets centerlinje.

**Nyckelord:** tröghetsbehäftad suspension, reologi, icke-Newtonska fluider, viskoelastik, sedimentering, deformerbara partiklar, hyperelastik.

## Preface

This PhD thesis deals with the numerical study of the behavior of finite-size particle suspensions in Newtonian and non-Newtonian fluids in different flow cases. A brief introduction on the involved physics and methods is presented in the first part. The second part contains four articles. The papers are adjusted to comply with the present thesis format for consistency, but their contents have not been altered as compared with their original counterparts.

**Paper 1.** D. Alghalibi, I. Lashgari, S. Hormozi and L. Brandt , 2018. *Interface-resolved simulations of particle suspensions in Newtonian, shear thinning and shear thickening carrier fluids.* J. Fluid Mech. **852**, 329–357.

**Paper 2.** D. Alghalibi, M. E. Rosti and L. Brandt, 2019. *Interface-resolved simulations of particle suspensions in visco-elastic carrier fluids.* Submitted to J. Fluid Mech..

**Paper 3.** D. Alghalibi, W. Fornari, M. E. Rosti and L. Brandt, 2019. *Sedimentation of finite-size particles in quiescent wall-bounded shear-thinning and Newtonian fluids.* International Journal of Multiphase Flow, under first review.

**Paper 4.** D. Alghalibi, M. E. Rosti and L. Brandt, 2019. *Inertial migration of a deformable particle in pipe flow.* Physical Review Fluids **4** (10), 104201.

December 2019, Stockholm
*Dhiya Abdulhussain Alghalibi*

**Division of work between authors**

The main advisor for the project is Prof. Luca Brandt (LB).

**Paper 1.** The computations have been performed by Dhiya Alghalibi (DA) using the code modified by Iman Lashgari (IL). Data analyses have been done by DA with the help from IL. The paper has been written by DA and Sarah Hormozi with feedback from IL and LB.

**Paper 2.** The computations have been performed by DA using the code modified by Marco Edoardo Rosti (MER). Data analyses have been done by DA. The paper has been written by DA and MER with feedback from LB.

**Paper 3.** The computations have been performed by DA using the code modified by Walter Fornari (WF). Data analyses have been done by DA with the help from WF. The paper has been written by DA and revised by MER and WF with feedback from LB.

**Paper 4.** The computations have been performed by DA using the code developed by MER. Data analyses have been done by DA with the help from MER. The paper has been written by DA and MER with feedback from LB.

# Contents

**Abstract** v

**Sammanfattning** vii

**Preface** ix

**Part I - Overview and summary**

**Chapter 1. Introduction** 1
1.1. Aim of the current study 7

**Chapter 2. Non-Newtonian fluid models** 9
2.1. Inelastic fluid models 10
2.2. Visco-elastic fluid models 11

**Chapter 3. Rigid particle-laden flows** 14
3.1. Navier-Stokes and Newton-Euler equations 14
3.2. Numerical method for rigid particle-laden flows 15
3.3. Volume penalization IBM 23

**Chapter 4. Deformable hyper-elastic particles in a flow** 26
4.1. Governing equations 26
4.2. Numerical method 27

**Chapter 5. Summary of the papers** 30

**Chapter 6. Conclusions and outlook** 33
6.1. Concluding remarks 33
6.2. Outlook 37

**Acknowledgements** 38

**Bibliography** 39

**Part II - Papers**

**Paper 1.** **Interface-resolved simulations of particle suspensions in Newtonian, shear thinning and shear thickening carrier fluids** 55

**Paper 2.** **Interface-resolved simulations of particle suspensions in visco-elastic carrier fluids** 91

**Paper 3.** **Sedimentation of finite-size particles in quiescent wall-bounded shear-thinning and Newtonian fluids** 125

**Paper 4.** **Inertial migration of a deformable particle in pipe flow** 155

# Part I

# Overview and summary

Chapter 1

# Introduction

Suspensions of solid/deformable particles in fluids are found almost everywhere in our lives from natural and geophysical to biological and industrial flows. Environmental phenomena cover pyroclastic flows from volcanoes, avalanches, sedimentation flows in river bed, dust storms, cloud and planetary flows as well as different biological flows such as blood cells flow in vessel, and the motion of suspended micro-organisms in water (e.g. plankton). Particle suspensions also occur in various industrial applications including food industries, particulate flows in fluidized beds, slurry transportation, oil-well drilling and pulp fibers in paper making (see figure 1.1). Often, in these particulate flows, the carrier fluid might exhibit non-Newtonian behaviors where the relation between the applied shear stress and shear-rate in the flow is no longer linear and instantaneous, opposite to the behavior of the Newtonian fluids, and the governing equations of the flow motion are more sophisticated as they account for these differences. This wide range of applications motivates many scientists to study the behavior of the complex flows from both microscopic and macroscopic point of views to advance our knowledge about these flows.

Non-Newtonian fluids may display numerous peculiar behaviors, such as shear-thinning, shear-thickening, elasticity and memory effects under different conditions. Shear-thinning and shear-thickening fluids show an apparent viscosity which decreases and increases with the applied shear rate. Elastic effects characterize the trend of the complex structures to relax back to their original configurations after being stretched by the flow. Memory effect has a close link to the fluid elasticity, but also to the short-range interactions among the particles defining the microstructure. The flow may remember the history of its past deformation over a duration specified by the relaxation time.

Differently from a single phase flow where, for example, the pressure drop can be precisely predicted as a function of the Reynolds number, $Re$, which is defined as the ratio between inertial to viscous effects of the flow (Pope 2000) and of the wall surface properties such as roughness and permeability (Orlandi & Leonardi 2008; Rosti *et al.* 2018*b*), it is still complicated to estimate the force needed to drive suspensions in spite of the numerous studies that have exposed various complex features of suspension flows, the origin of many of which are not yet fully understood (see Stickel & Powell 2005). The complexities

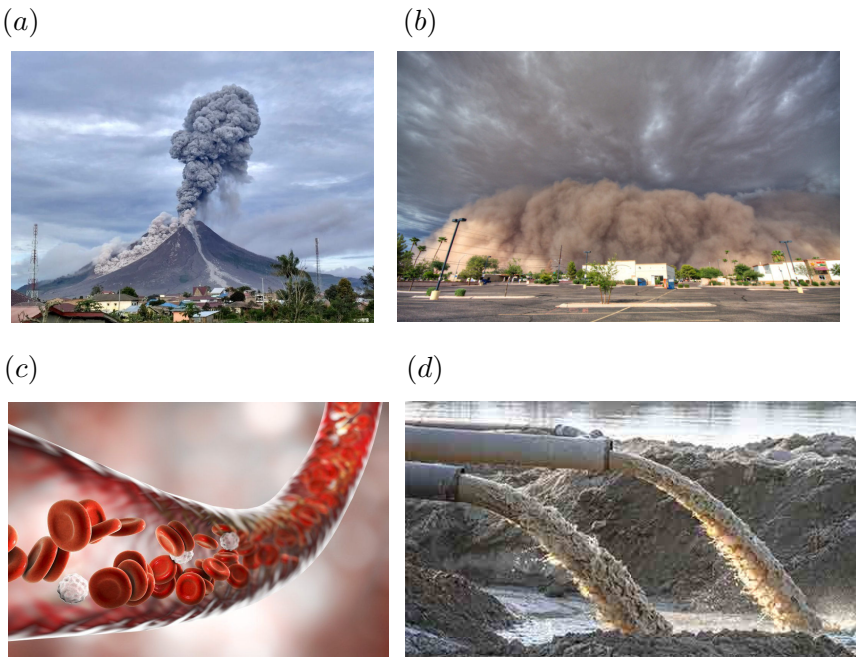


Figure 1.1: Examples of particle laden flows (a) Pyroclastic flows from the Sinabung volcano, Indonesia, 2017 (source: www.volcanodiscovery.com); (b) a giant dust storm ready to engulf Gilbert, Arizona, a suburb of Phoenix, 2018 (source: epod.usra.edu); (c) lipid and red blood cells flowing through vessels (source: finance.yahoo.com); (d) slurry transportation (source: www.rdi.uwa.edu.au).

and challenges of multiphase flows are mainly due to the numerous additional parameters such as the physical properties of the particles (e.g., shape, size, stiffness, density difference with suspended fluid, solid volume fraction), the large set of interactions among particles (e.g., hydrodynamic, contact, inter-particle forces) and the properties of the carrier fluid (Newtonian or non-Newtonian); variations of each of these parameters may provide substantial quantitative and qualitative changes in the behavior of the suspension and affect the overall dynamics in several and sometimes surprising ways (Mewis & Wagner 2012). This makes the problem of particle suspension multidimensional. From a mathematical point of view, the complexity in dealing with these suspensions arises from the fact that it is necessary to solve the governing equations of the carrier fluid (continuum) phase, often the Cauchy or Navier-Stokes and continuity equations, with those of the dispersed (particle) phase as well as appropriate boundary conditions on the surface of each particle (the interface between the two phases).

In the following paragraphs, a general introduction about particles dispersed in a viscous fluid flows is presented to provide the reader with a brief idea of the broad range of applications of particulate flows and about the complexity of the problem.

**Particles dispersed in simple shear flows**

Starting from the simpler case of particles dispersed in a viscous fluid, the macroscopic behavior of mono-disperse rigid neutrally-buoyant spherical particle suspensions in a Newtonian carrier fluid has been the object of many previous studies, the main objective being the the measurement of the suspension shear viscosity (effective viscosity). The bulk stress of the particle suspensions is affected by the particle stresslet (i.e., the stress from the particle that resists the flow deformation Batchelor 1970). Thus, the effective viscosity primarily depends on the volume fraction of the dispersed phase, $\Phi$, more so in the Stokesian regime when the inertial effects are negligible, i.e., $Re_p = \rho_f \dot{\gamma} a^2/\mu \to 0$ (where $\rho_f$ is the fluid density, $\dot{\gamma}$ the flow shear rate, $a$ the particle radius and $\mu$ the fluid viscosity). In inertial suspension inertia plays a role not only at bulk level but also at the particle scale and the particle Reynolds number, $Re_p$, is non-zero. Note that in our study, we have suspensions made out of larger particles ($a \gg 10$ $\mu$m); i.e. the suspensions are non-colloidal and Brownian motion does not affect the particle motion. This condition occurs in many applications, such as slurry transport, where the typical particle size is between (100-1000 $\mu$m) much larger than the size of the colloidal particles, which is about 1 $\mu$m (Jeffrey & Acrivos 1976).

In the Stokesian regime, the movement of an isolated particle is typically fully reversible and there is a linear relationship between the particle velocity and the drag force acting on it. It is noteworthy to mention that irreversible dynamics is found in suspensions, due to the combined effects of interactions among particles such as non-hydrodynamic (e.g., collisions, roughness) and hydrodynamic interactions (Guazzelli & Morris 2011*a*). If the concentration is low, the suspension is dilute, the stresslet is almost the same for each particle additive, which means that the bulk stress increases linearly with the volume fraction. In this case, the suspension shear viscosity follows the linear formulation first suggested by Einstein (1906, 1911) $\mu_{eff} = \mu\,(1 + 2.5\Phi)$ where interactions between particles are neglected; at higher concentration the quadratic formulation by Batchelor (1977) $\mu_{eff} = \mu\left(1 + 2.5\Phi + 6.95\Phi^2\right)$ is a good approximation because reciprocal interactions of particle are included. As the particle concentration increases, the behavior of the suspensions becomes more complex due to the multi-body and short-range interactions and the effective viscosity can no longer be predicted with analytical methods, and empirical fits are commonly used; these are obtained in the form of an increasing function of the volume fraction diverging at the maximum packing fraction, such as those by Eilers and Krigher & Dougherty (see for more details the review by Stickel & Powell 2005). The usual empirical fits are no longer valid if inertia

at the scale of particles becomes important (i.e., when the particle Reynolds number $Re_p$ is finite), and the rheological observables may significantly vary from those in the Stokesian regime, i.e. the relation between drag force and velocity becomes nonlinear for an isolated particle, (see for example, the recent numerical studies by Kulkarni & Morris 2008*a*; Picano *et al.* 2013; Yeo & Maxey 2013). In particular, the study of Picano *et al.* (2013) shows that the inertia affects the suspension microstructure, resulting in an enhancement of effective shear viscosity. As $Re_p$ increases, the pair distribution function, quantifying the particle relative position during flow, becomes more anisotropic, almost zero on the rear of the particles, effectively reproducing additional excluded volumes. This anisotrpy increases the effective solid volume fraction, and consequently, the effective shear viscosity. Taking into account this excluded volume effect (which depends on both $\Phi$ and $Re_p$), Picano *et al.* (2013) scaled the effective shear viscosity in presence of small inertia to that of Stokesian suspensions.

The behavior of suspensions is even more complex when the carrier fluid is non-Newtonian, such as generalized Newtonian (when the viscosity is a complex function of the applied shear, yet the response instantaneous) or visco-elastic fluids. Only a few studies have been devoted to non-colloidal particles suspended in non-Newtonian fluids, attempting to address the bulk rheology from a continuum-level closure perspective. These studies mainly focus on non-inertial suspensions with few exceptions (see for example the work by Hormozi & Frigaard (2017)). When the carrier fluid is visco-elastic, as upon addition of polymers, the resulting stresses are altered by two main mechanisms: (*i*) the surface traction change, hence the stresslet contribution may also change and (*ii*) the solid phae induces additional fluid stress because of the polymers stretching in the gradients of flow induced by the particles (Yang *et al.* 2016). This can lead to unexpected behaviors, such as particle alignment during sedimentation (Joseph *et al.* 1994) or chain formation during shear flow (Michele *et al.* 1977; Lyon *et al.* 2001; Scirocco *et al.* 2004). So far, only few numerical studies have focused on particle suspensions in visco-elastic fluids, focussing on the dilute regime (Yang *et al.* 2016; Yang & Shaqfeh 2018*b*,*a*). To the best of our knowledge, no other 3D numerical simulations of the rheology of particle suspensions in visco-elastic fluids exist in literature which explored a wider range of particle concentrations, polymer relaxation time and applied shear-rate.

**Sedimentation**

Concerning the settling of particles under the action of gravity in a narrow channel, the sedimentation of an isolated spherical and non-spherical particle through Newtonian and non-Newtonian fluids has been extensively examined in the past, (see for example the references Clift *et al.* 2005; Chhabra 2006). The earliest investigations of the sedimentation focussed however on a single rigid sphere in an unbounded quiescent Newtonian fluid, considered Stokes flow, where the particle terminal velocity is linked to the particle radius, the difference between the solid and fluid density and the fluid viscosity. Since then,

several studies extended the Stokes law by investigating the effects of additional parameters such as the presence of non-Newtonian media, different particle shapes, inertia, and soon interactions between particles and the effect of walls (e.g. Shah *et al.* (2007); Putz *et al.* (2008); Zhang *et al.* (2016)).

When the concentration of particles is further increased, the trajectory and settling velocity of an individual sedimenting object is affected by the presence of the others: this leads to a decrease of the mean settling velocity of the suspension, due to the so-called hindering effect (Davis & Acrivos 1985). The hindering effect monotonically increases as a function of the solid volume fraction $\Phi$, hence, the mean settling velocity is monotonically decreasing with $\Phi$. The behavior of many particles settling in a complex fluid is a less studied problem (Izbassarov *et al.* 2018). Only a few experimental and numerical studies have been devoted to the sedimentation of particle suspensions in quiescent non-Newtonian fluids, and the topic remains therefore poorly understood. It was observed in experimental investigations in the Stokesian regime that the settling particles cluster to form columns or chains and cause the development of non-homogeneous structures during the sedimentation in either a shear-thinning fluid (Allen & Uhlherr 1989; Bobroff & Phillips 1998; Daugan *et al.* 2004) or a viscoelastic fluid (Allen & Uhlherr 1989; Joseph *et al.* 1994; Bobroff & Phillips 1998). In addition, the aggregation of the particles has been numerically examined in a viscoelastic fluid (Yu *et al.* 2002) and in a thixotropic shear-thinning fluid (an inelastic shear-thinning fluid with memory) (Yu *et al.* 2006*a*).

**Particle migration**

The presence of solid walls induces interesting particle migration phenomena, such as particle separation (Lim *et al.* 2014) and focusing (Lu *et al.* 2017). These phenomena have been successfully applied for the manipulation of particles and cells in microfluidic devices. In a Newtonian fluid flow, the two most important non-dimensional parameters characterizing the motion of deformable particles are the Reynolds $Re$ and Weber $We$ numbers (or capillary number), quantifying inertia and particle elasticity, respectively. The Weber number $We$ is defined as the ratio of inertia to elastic effects acting on the deformable particle. Generally, in the absence of inertia, a neutrally buoyant rigid sphere follows the fluid motion without any lateral migration in order to satisfy the reversibility property of the Stokes flow (Guazzelli & Morris 2011). On the other hand, deformable particles in the same condition move towards low shear gradient regions, hence, when suspended in a Poiseuille flow they migrate towards the center of the channel (Kaoui *et al.* 2008). In inertial flows, the trajectories of both rigid and deformable particles do not necessarily follow the behavior observed in the Stokes regime and particles undergo lateral migration. This is the case for typical inertial microfuidics applications ($Re > 1$ and $We > 0$), when inertial and elastic forces dominate the cross-streamline migration and determine the final equilibrium position of the particles. In particular, elasto-inertial microfluidics is emerging as a powerful tool and research area, with devices where elasticity and inertia

are being engineered to achieve efficient particle focusing and/or particle sorting (Stoecklein & Di Carlo 2018).

Lateral migration and focusing of rigid particles were first observed experimentally in a Newtonian circular pipe flow by Segre & Silberberg (1961). In a pipe flow, initially randomly distributed neutrally buoyant spheres immersed in a Newtonian carrier fluid migrate radially and focus into a narrow annulus at around 0.6 the pipe radius, the so-called "tubular pinch" effect. Numerous studies exploited this process for microfluidics applications, described as "inertial focusing" of particles. Indeed, the equilibrium position of the particles is the net result of two opposing forces, resulting from the resistance of the solid particle to the deformation: *(i)* the shear gradient lift force, which is induced by the velocity profile curve, that directs the particle away from the channel centerline towards the wall and *(ii)* the wall-induced lift force arising from the interaction of the particle and the neighboring wall, which pushes the particle away from the wall towards the channel centerline (Martel & Toner 2014). These two competing forces, determining the lateral trajectory and the final equilibrium position of the particle, are modified differently by the blockage ratio (Di Carlo 2009) and the flow Reynolds number (Matas *et al.* 2004), and thus, by properly designing the geometry of the microfluidic device, the lateral motion can be used for cell focusing, separation, trapping, sorting, enrichment and filtration (see the review articles by Di Carlo (2009) and Karimi *et al.* (2013)).

When the particle is deformable, the dynamics is further complicated by an additional force called "deformation-induced lift force" arising from the deformation of the particle shape itself, which moves the particle towards the centerline and which becomes stronger as the particle deformation increases (Raffiee *et al.* 2017; Hadikhani *et al.* 2018). It is worth noting that the alterations of the particle shape also affect and modify the two forces discussed previously, making the problem fully coupled. During the last 10 years, the dynamics of deformable particles have been studied both experimentally and numerically (e.g., Mach & Di Carlo 2010; Hur *et al.* 2011; Kim *et al.* 2015; Wang *et al.* 2016). In particular, Hur *et al.* (2011) showed that particles can be separated depending on their size and elastic deformability; same behavior was also observed in numerical simulations (Kilimnik *et al.* 2011; Chen 2014). In spite of the fact that all the results indicate that the soft deformable particles move to the channel centerline, the effect of the flow Reynolds number is not quite understood and still debated.

Most of the previous works on the dynamics of deformable particles in Newtonian flows in cylindrical straight pipes have mainly focused on the low Reynolds number regimes. In addition, it is challenging to capture in experiments the entire migration dynamics of a deformable particle, such as its trajectory, the deformed shape and the forces acting on the particle.

## 1.1. Aim of the current study

From the above introduction, one may conclude that many experimentally and numerically observed behaviors are still far from clear; given the wide range of parameters involved there is still much to explore in each of the different flow regimes and in different non-Newtonian fluid types. In addition, the combined effects of the non-Newtonian properties of the suspending fluid, such as shear-thinning, shear-thickening and visco-elastic effects, with a dispersed solid phase at moderate and high volume fractions makes the dynamics of such flows, which are mostly unexplored, extremely complex. Because of these complexities and challenges, our general understanding of the problem is still incomplete. Therefore, the aim of this work is to use interface-resolved numerical simulations to provide a deeper understanding of the behavior of suspensions in laminar Newtonian and non-Newtonian (inelastic and/or visco-elastic) fluid flows for a wide range of different parameters, including the effect of physical and mechanical properties of the particles and the fluid that surrounds them. The fully-resolved simulations improve our fundamental understanding by providing access to the local values of fluid and solid phase velocities, solid volume fraction and shear rate, i.e. it is possible to obtain new insight on the interactions among the different phases and the resulting transport mechanisms and suspension microstructure. However, given their costs, simulations are limited to some selected cases, often in simple canonical configurations, so that a wider parameter space can be inevitably covered by experiments. Moreover, short-range particle interactions/collisions as well as the properties of the carrier fluid need to be assumed and modelled. Nevertheless, we hope this thesis shows that by judiciously choosing the simulation setup new fundamental understanding can be obtained from the analysis of the numerical data. In particular, in the present work, to fill in the literature gaps as discussed previously, it was of special to answer the following research questions:

- For inelastic non-Newtonian carrier fluids, can the suspension shear viscosity be predicted by the homogenization theory of Chateau *et al.* (2008) in Stokesian regime at a wide range of volume fraction? Is it still valid when adding inertia to the system?
- How will the visco-elastic and shear-thinning effects alter the microstructure and rheology of the suspensions at moderate and high volume fraction and fluid elasticity?
- What is the role of inertia on the rheology of particle suspensions with different types of fluids?
- What is the effect of a shear-thinning fluid on the settling behavior of suspensions in a quiescent wall-bounded environment with finite particle Reynolds number at moderate and high volume fractions?
- What are the effects of inertia and elasticity of a deformable particle on the migration dynamics and the equilibrium position?

To assess these questions appropriate methodologies are required. In this work, we have employed efficient numerical methods to study particle suspensions in different non-Newtonian fluids. The models used to represent some of the non-Newtonian features of complex fluids and the numerical methods adopted are explained and discussed in the next chapters. In particular, two inelastic and two visco-elastic non-Newtonian models employed in this work are introduced in chapter 2. The governing equations and numerical method used to simulate the suspension of finite size rigid particles are given in chapter 3, followed by chapter 4, where the governing equations for the motion of a single deformable viscous hyper-elastic particle suspended in a Newtonian fluid flow are discussed together with the numerical method used here. Finally, in chapter 5 and 6 the main results and conclusions are summarized and an outlook on possible future works is provided. The thesis work resulted in four papers, which are all included in the back.

Chapter 2

# Non-Newtonian fluid models

Unlike Newtonian fluid, e.g. water and oil, many of the fluids usually dealt with in industrial applications are non-Newtonian in behavior due to the existence of macromolecular complex structures suspended or dissolved in the liquid. Among these we recall gels, blood, paints, colloidal suspensions and polymer solutions. In Newtonian fluids, having isothermal and incompressible flow, the fluid shear stress is linearly dependent on the applied strain rate with a constant coefficient that is called fluid viscosity. On the contrary, non-Newtonian fluids may reveal a nonlinear relationship between the fluid stress and an applied shear rate (Bird *et al.* 1987). The interactions between the macromolecular structures in non-Newtonian fluids are very complex in many rheologically interesting systems hence, the chemical and physical properties of these liquids cannot be easily modelled. As an alternative, constitutive equations are derived based on the continuum mechanics to predict the non-Newtonian fluid behaviors. Different constitutive equations can be used to classify the systems into inelastic and elastic fluids. In the inelastic fluid models, e.g. Carreau, Power-law and Bingham models, the focus is mostly on the instantaneous change of the fluid viscosity with the applied shear rate. These models are comparatively simple to be utilized in the numerical and analytical investigations, however, they cannot capture all the features of the different non-Newtonian fluids such as memory and elasticity effects. In the elastic fluid models, e.g. Maxwell, Oldroyd-B, Giesekus and FENE-P models, the fluid stress does not change instantaneously with the shear rate to account for the memory effect of the flow. To model visco-elastic non-Newtonian fluids, often the viscous and elastic effects are put together based on an identical principle as a mechanical system including dashpots and nonlinear elastic spring (Morrison 2001). In spite of the fact that the non-Newtonian models are idealized, they can capture the different behaviors of various real fluids under specific conditions. In the current study, we employ the Carreau, power-law, Oldroyd-B and Giesekus models to investigate the shear-thinning, shear-thickening and visco-elastic effects of non-Newtonian fluids on a rigid particle suspensions. These models describe the viscosity and stress well-enough for most engineering computations (Bird *et al.* 1987).

## 2.1. Inelastic fluid models

When the fluid flows are governed by effects of the fluid viscosity, then it makes sense to model the fluid viscosity function precisely. Inelastic, or generalised Newtonian, fluid models describe the behavior of purely viscous fluids, where the extra fluid stress tensor, $\boldsymbol{\tau}$, is proportional to the instantaneous flow deformation rate tensor, but the coefficient of proportionality (the fluid viscosity), $\mu_f$, is allowed to depend on the instantaneous flow shear rate:

$$\boldsymbol{\tau} = 2\mu_f(\dot{\gamma})\boldsymbol{\Theta}, \tag{2.1}$$

where $\boldsymbol{\Theta}$ is the symmetric part of the velocity gradient tensor ($\boldsymbol{\Theta} = \frac{1}{2}(\nabla\mathbf{u} + \nabla\mathbf{u}^T)$). The second invariant of the strain-rate tensor is indicated as $\dot{\gamma}$ and is computed by the dyadic product, $\dot{\gamma} = \sqrt{2\{\Theta_{ij} : \Theta_{ij}\}}$, (see Bird *et al.* 1987).

### 2.1.1. *Shear-thinning fluid model*

Shear thinning (pseudoplastic), the decrease of fluid viscosity with flow shear rate, is a popular behavior and is exhibited by paints, concentrated polymer solutions, and dispersed systems such as emulsions, inks and latex (Braun & Rosen 2013). Various forms for the viscosity have been suggested for these fluids; the most common one is the Carreau model. This model supposes anisotropic viscosity proportional to some power of the instantaneous flow shear rate $\dot{\gamma}$ (Morrison 2001),

$$\mu_f(\dot{\gamma}) = \mu_\infty + \frac{\mu_0 - \mu_\infty}{(1 + \lambda_c^2\dot{\gamma}^2)^{(1-n)/2}}. \tag{2.2}$$

In this equation, there are four parameters: $\mu_\infty$ is the lower limit of the fluid viscosity at infinite-shear-rate, $\mu_0$ is the upper limit of the viscosity at zero-shear-rate, $\lambda_c$ is a time constant that represents the degree of shear-thinning (this constant has no relation to the relaxation time of the fluid) and its magnitude can be connected to the molecular structure of several polymeric solutions (Morrison 2001; Phan-Thien & Mai-Duy 2017), and $n$ is called the power-index which characterizes the fluid behavior. For $0 < n < 1$ the fluid is shear thinning. For $n = 1$, the model represents the Newtonian fluids where the viscosity becomes independent of the shear-rate.

### 2.1.2. *Shear-thickening fluid model*

The behavior of the shear thickening (dilatant) fluids, where the viscosity increases reversibly as the applied shear rate increases, is not as common as shear thinning. Examples of dilatant fluids are corn starch solution, suspensions of concentrated clay, glass rods suspensions (Braun & Rosen 2013), ceramic suspensions (casting slurries), dental dilling masses (dental composites) and special composite materials for protective clothing (Mezger 2015). For these type of fluids, we utilize the Power-law model to calculate the fluid viscosity,

$$\mu_f(\dot{\gamma}) = m\dot{\gamma}^{n-1}, \tag{2.3}$$

which creates a monotonic increase of the fluid viscosity with the local shear rate when $n > 1$. The constant $m$ is called the consistency index and denotes the slope of the viscosity profile. This model also can describe the Newtonian fluids. In that case $n = 1$ and $m = \mu_f$. However, the major disadvantage of this model is that it collapses in zones where the local shear rate tends to zero - in these zones the fluid viscosity is infinite, and regularization might be necessary.

## 2.2. Visco-elastic fluid models

Many polymeric fluids are also called visco-elastic fluids (e.g., Molten polymers, shampoos, glues, eggs white, Bouncing Putty and offset printing inks). This means that the fluids display a mixture of viscous and elastic behavior when sheared. Viscous properties are associated with the appearance of irreversible deformations that enhance with time and stay upon removal of the stress. On the other hand, elastic properties relate to the occurrence of reversible deformations as in a solid, which vanish automatically and directly upon removal of the stress. However, the prevalence of the elastic or viscous behavior depends on the time scale of the applied deformation. Generally, it can be concluded that a more quick deformation of the material relates to larger elasticity, and in an opposite way, a slower deformation triggers a viscous response of the material. These properties rely on the macromolecular structure, the existence of particles, and interactions of particles in the investigated material (Izdebska & Thomas 2015). The relative visco-elastic effect, i.e. the ratio of elastic to viscous forces, is usually measured by the dimensionless Weissenberg number $Wi$, calculated by the product of a characteristic relaxation time $\lambda_m$ of the material and a characteristic deformation rate $\dot{\gamma}$ of the flow:

$$Wi = \lambda_m \dot{\gamma}. \tag{2.4}$$

Different models have been developed to capture the visco-elastic behavior of some common non-Newtonian fluids. In the current study, we use the quasi-linear Oldroyd-B model to consider a purely elastic fluid, although this model is not physical consistent as it allows an infinite stretching of the polymer chains, and the non-linear Giesekus model for the combined shear-thinning and elastic effects. Both models can be derived from kinetic theory (Izdebska & Thomas 2015), assuming that polymer molecules behave like a suspenshon of Hookean dumbbells (i.e. two beads connected with an elastic spring) in a Newtonian solvent (Giesekus 1982; Tirtaatmadja & Sridhar 1995; Zhu *et al.* 2012). For these two constitutive models, the total deviatoric stress tensor, $\boldsymbol{\tau}$, can be split into a purely viscous contribution, corresponding to the instantaneous response of the solvent, and a polymeric contribution, accounting for the microsturcture memory:

$$\boldsymbol{\tau} = \boldsymbol{\tau}_s + \boldsymbol{\tau}_m. \tag{2.5}$$

The solvent stress is defined as,

$$\boldsymbol{\tau}_s = 2\mu_s \boldsymbol{\Theta}, \tag{2.6}$$

where $\mu_s$ is the solvent viscosity (i.e. the Newtonian part), while the instantaneous values of all the components of the additional visco-elastic stress tensor $\boldsymbol{\tau}_m$ are found by solving the objectives and frame-independent transport equations discussed below, which depend on the constitutive models considered here (for more details, see Giesekus 1982; Larson 1988).

### 2.2.1. *Oldroyd-B fluid model*

The Oldroyd–B (or Upper convected Jeffreys) fluid model, originally proposed by Oldroyd (1950), is used to describe the flow of constant-viscosity elastic fluids, where the fluids behave like a dilute solution of polymer molecules modeled as Hookean dumbbells (Bird *et al.* 1987). The Oldroyd–B constitutive equation for the polymeric stress $\boldsymbol{\tau}_m$ is written as:

$$\boldsymbol{\tau}_m + \lambda_m \boldsymbol{\tau}_m^{\triangledown} = 2\mu_m \boldsymbol{\Theta}. \tag{2.7}$$

In this equation, $\mu_m$ is the polymeric viscosity (i.e. the non-Newtonian part) and $\boldsymbol{\tau}_m^{\triangledown}$ denotes the upper convected time derivative of $\boldsymbol{\tau}_m$, and is defined by

$$\boldsymbol{\tau}_m^{\triangledown} = \frac{\partial \boldsymbol{\tau}_m}{\partial t} + \mathbf{u} \cdot \nabla \boldsymbol{\tau}_m - \nabla \mathbf{u}^T \cdot \boldsymbol{\tau}_m - \boldsymbol{\tau}_m \cdot \nabla \mathbf{u}. \tag{2.8}$$

Note that, the total viscosity of the visco-elastic fluid is the sum of the solvent and the polymeric viscosities, i.e. $\mu_f = \mu_s + \mu_m$. This model is no longer linear because the convected derivative terms introduce nonlinear terms in the velocity gradient $\nabla \mathbf{u}$ (Morrison 2001), and for this reason Bird *et al.* (1987) call it quasi-linear. In a steady state simple shear flow, this model predicts a constant viscosity of the visco-elastic fluid and a first-normal stress difference which is quadratically dependent on shear rate over a large shear rate range, as well as zero second normal-stress difference. The Oldroyd-B model characterizes many features of the so-called Boger fluids, fluids that show constant viscosity but also pronounced normal-stress effects (Phan-Thien & Mai-Duy 2017). Hence, the Oldroyd-B model has been utilized extensively to study these pure elastic fluids in many flow cases, both theoretically and numerically (Tirtaatmadja & Sridhar 1995).

### 2.2.2. *Giesekus fluid model*

The Giesekus model has been derived by Giesekus (1982) from the kinetic theory of concentrated polymer solutions. The constitutive equation of this model contains a nonlinear stress term, including a dimensionless mobility factor $\alpha$ which is connected with the anisotropic hydrodynamic drag and/or anisotropic Brownian motion on the constituent polymer molecules (Bird & Wiest 1985):

$$\boldsymbol{\tau}_m + \lambda_m \boldsymbol{\tau}_m^{\triangledown} + \frac{\lambda_m \alpha}{\mu_m} (\boldsymbol{\tau}_m \cdot \boldsymbol{\tau}_m) = 2\mu_m \boldsymbol{\Theta}. \tag{2.9}$$

The presence of the nonlinear stress term in the Giesekus model gives shear flow properties which vary with shear rates. Based on thermodynamic conditions and realistic properties, $\alpha$ must be in the range between 0 and 0.5 (Schleiniger & Weinacht 1991), where the model predicts a shear-thinning behavior, namely, the polymeric viscosity decreases monotonically with the shear-rate, with the mobility factor controlling such effect: the larger $\alpha$, the more pronounced is the shear-thinning. On the contrary, when $\alpha = 0$, the polymer has a constant viscosity and the the Giesekus constitutive equation reduces to the Oldroyd-B constitutive equation (2.7). Note that, in a simple shear flow, the total fluid viscosity at zero shear-rate, $\mu_f|_{\dot{\gamma}=0}$, is equal $(\mu_s + \mu_m)$. In general, at any value of an applied shear-rate, the total fluid viscosity, $\mu_f$ is calculated as,

$$\mu_f(\dot{\gamma}) = \mu_s + \frac{\tau_{m12}}{\dot{\gamma}}. \tag{2.10}$$

Here, $\tau_{m12}$ is the polymer shear stress component. The model also predicts non-zero first and second normal stress differences, defined below, which can lead to flow phenomena very peculiar of non-Newtonian fluids (e.g. rod climbing effect).

$$N_1 = \tau_{m11} - \tau_{m22}, \tag{2.11}$$

$$N_2 = \tau_{m22} - \tau_{m33}, \tag{2.12}$$

where $\tau_{m11}$, $\tau_{m22}$ and $\tau_{m33}$ denote the normal stress along $x$, $y$ and $z$ directions, respectively. A more in-depth discussion of these models can be found in Bird *et al.* (1987) and Larson (1988).

Chapter 3

# Rigid particle-laden flows

In this chapter, the governing equations for suspensions of finite size rigid particles in Newtonian and different types of non-Newtonian carrier fluid models are discussed. Then, we continue with the numerical approaches to resolve this problem and finally we introduce the volume penalization IBM which is considered in this thesis to model the flow in a circular pipe, still using a cartesian mesh..

## 3.1. Navier-Stokes and Newton-Euler equations

In a system of rigid particles suspended in a fluid, the dynamics of both solid and fluid phases are fully coupled. The motion of the particles is determined by the hydrodynamic forces and moments applied on them via the surrounding fluid. On the other hand, the fluid motion is substantially affected by the motion of the particles and, as in the sedimentation case, even entirely driven by the particle motion.

Generally the carrier fluid is dealt with as a continuum of an infinite number of fluid particles. Each particle of fluid contains of a large number of individual molecules or atoms and is described by its averaged properties (e.g., velocity, pressure, temperature, density and other important quantities). In this way, we are able to determine these properties at each point of the fluid. In addition, when the flow velocity is significantly smaller than the velocity of sound (less than 30%), the fluids (liquids or gases) can be further supposed to be incompressible (i.e., the total volume of each fluid particle is always fixed). In many applications, $Re_p \neq 0$, and thus the inertia of both the fluid and the particles has to be considered in the model. The final set of governing equations describing the dynamics of these fluids, Newtonian and non-Newtonian suspended fluids, is well known as the incompressible Cauchy momentum and continuity equations,

$$\rho_f \left( \frac{\partial \mathbf{u}}{\partial t} + \mathbf{u} \cdot \nabla \mathbf{u} \right) = \nabla \cdot \boldsymbol{\sigma} + \rho_f \mathbf{f}, \tag{3.1}$$

$$\nabla \cdot \mathbf{u} = 0. \tag{3.2}$$

In these equations $\mathbf{u} = (u, v, w)$ is the velocity vector with components in the $(x, y, z)$ coordinate directions. The density of fluid is indicated by $\rho_f$, while the body force $\mathbf{f}$ indicates the forcing from the dispersed phase on the carrier fluid used to impose the boundary conditions on the solid boundaries through an Immersed Boundary Method (IBM) in our implementation. Finally, the stress tensor $\boldsymbol{\sigma}$ is decomposed into a pressure $P$ and a viscous part (deviatoric stress) $\boldsymbol{\tau}$:

$$\boldsymbol{\sigma} = -P\mathbf{I} + \boldsymbol{\tau}, \tag{3.3}$$

in which $\mathbf{I}$ is the identity tensor. The total deviatoric stress tensor, $\boldsymbol{\tau}$, is calculated by using various non-Newtonian fluid models as defined previously in chapter 2.

The motion of the rigid spherical particles is described by the Newton-Euler equations,

$$\rho_p V_p \frac{\mathrm{d}\mathbf{U}_c^p}{\mathrm{d}t} = \oint_{\partial V_p} \boldsymbol{\sigma} \cdot \mathbf{n} dS + (\rho_p - \rho_f) V_p \mathbf{g} + \mathbf{F}_c, \tag{3.4}$$

$$I_p \frac{\mathrm{d}\boldsymbol{\omega}_c^p}{\mathrm{d}t} = \oint_{\partial V_p} \mathbf{r} \times \boldsymbol{\sigma} \cdot \mathbf{n} dS + \mathbf{T}_c, \tag{3.5}$$

where $\mathbf{U}_c^p$ and $\boldsymbol{\omega}_c^p$ are center velocity and rotation rate of the particle $p$, while $\rho_p$, $V_p = 4\pi a^3/3$ and $I_p = 2\rho_p V_p a^2/5$ are the mass density, volume and moment-of-inertia of a sphere with radius $a$. In these equations, $\partial V_p$ represents the surface of the particles with outwards normal vector $\mathbf{n}$, $\mathbf{g}$ is the gravitational acceleration, the radial distance from the center to the surface of each particle is indicated by $\mathbf{r}$. The force and torque, $\mathbf{F}_c$ and $\mathbf{T}_c$, act on the particle as a result of particle-particle or particle-wall collisions, and typically need to be modelled in numerical simulations. The no-slip and no-penetration boundary conditions on the particle surface are imposed by forcing the fluid velocity at each point on the surface of the particle, $\mathbf{X}$, to be equal to the velocity of the particle at that point, i.e., $\mathbf{u}(\mathbf{X}) = \mathbf{U}^p(\mathbf{X}) = \mathbf{U}_c^p + \boldsymbol{\omega}_c^p \times \mathbf{r}$. This condition is not imposed directly in the Immersed Boundary Method used in the current study, but instead included via the body force $\mathbf{f}$ on the right-hand side of equation (3.1).

## 3.2. Numerical method for rigid particle-laden flows

During the last decades, many viable numerical methods and algorithms have been proposed in the literature to implement interface-resolved direct numerical simulations (DNS) of rigid particle-laden flows. Among these numerical approaches, we can mention the *front tracking* method by Unverdi & Tryggvason (1992), several algorithms based on the *lattice Boltzmann* solver for the fluid phase (Ladd 1994*a*,*b*; Hill *et al.* 2001; Ten Cate *et al.* 2004), the *force coupling* approach by Lomholt & Maxey (2003), the *Physalis* method (Zhang &

Prosperetti 2005; Sierakowski & Prosperetti 2016) and the *Immersed Boundary* Method (IBM) (Peskin 1972; Uhlmann 2005; Breugem 2012). Needless to mention that each one of these approaches has its own advantages and disadvantages. Recently, in an overall review survey, Maxey (2017) reported the state-of-the-art algorithm and the principles and applications of each method.

For the scope of the present study, we use the IBM method due to its feasibility to exploiting efficient computational algorithms for solving the Navier-stokes equations on a Cartesian grid in the presence of numerous freely mobile finite-size rigid particles. In the following sections, the approach and the numerical treatments will be discussed in detail.

### 3.2.1. *Immersed Boundary Method (IBM)*

The immersed boundary method was first suggested by Peskin (1972) and several modifications and refinements have been developed since then, See (Mittal & Iaccarino 2005) for more details. Generally, as stated by Mittal & Iaccarino (2005), IBMs can be sorted into two main classes: continuous forcing or discrete (sometimes referred as direct) forcing approaches, which are based on the implementation of the extra force term $\mathbf{f}$ added to the governing equation 3.1. In the continuous forcing method, $\mathbf{f}$ is computed based on the velocity of the fluid at a point in the interface and the desired velocity at that point, hence, the the force is incorporated into the continuous momentum equations before discretization and the expression of the force does not depend on the numerical scheme, utilized to solve the Navier-Stokes equations. This approach is attractive for the simulation of elastic boundaries. The successful applications of the continuous forcing method can be found in many studies, e.g. Unverdi & Tryggvason (1992); Revstedt & Fuchs (2001); Zhu & Peskin (2003); Revstedt (2004, 2013). On the contrary, the discrete forcing approach is widely utilized to for rigid boundaries. In this method, the IB force is introduced after the governing equations are discretized, and its expression is thus dependent on the numerical scheme, utilized for discretization and solving momentum equations. This method is preferred, as it permits for a far better control over the numerical accuracy, stability, and conservation of the forces(the force should be conserved between the solid and fluid phases).

A computationally efficient discrete forcing method to fully resolve particle-laden flows was originally developed by Uhlmann (2005). This approach has been further modified by Breugem (2012), who proposed several refinements to make it second-order accurate in space by using a multi-direct forcing scheme (Luo *et al.* 2007) to better approximate the no-slip/no-penetration (ns/np) boundary condition on the particle surface and by applying a slight retraction of the grid points on the surface of the particle towards the interior. In addition, the numerical stability of this method for mass density ratios (solid-to-fluid density ratios) near unity, i.e. neutrally buoyant particle suspensions, was also improved by directly accounting for the inertia of the fluid contained within the immersed (virtual) boundaries of the particles (Kempe & Fröhlich 2012).

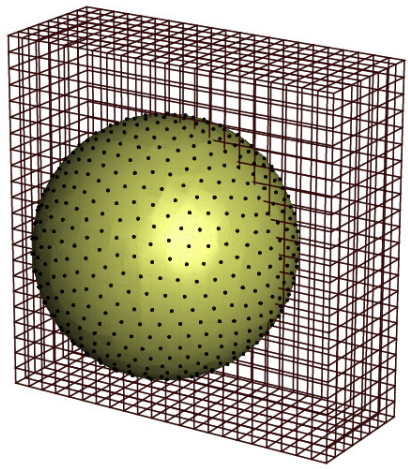

Figure 3.1: Skech of the quasi-2D Lagrangian and 3D Eulerian grids used in the immersed boundary approach. The Lagrangian grid points on the surface of the sphere are represented by small black dots; figure from (Breugem 2012).

This approach has been used extensively in several studies on finite size rigid particle suspensions for different Reynolds numbers (Lashgari *et al.* 2014), concentrations of particles (Picano *et al.* 2015), particle shapes (Ardekani *et al.* 2016), particle sizes (Costa *et al.* 2016), and mass density ratios (Fornari *et al.* 2016).

In the current work, The IBM version of Breugem (2012) is employed to simulate the motion of finite-size rigid particles suspended in different types of carrier fluids. The numerical code combines the flow solver for the Navier-Stokes equations with IBM to follow the motion of the suspended fluid and particles in the entire domain. In this method, the fluid field is described in an Eulerian framework on a uniform staggered, Cartesian grid ($\Delta x = \Delta y = \Delta z$) to solve the governing equations (3.1) and (3.2) on the whole domain, also inside the rigid particles. In the discretization, the velocity nodes are located on the cell faces, while fluid viscosity, the pressure and the extra stress components are all located at the cell centers. On the other hand, the solid phase, considering the governing equations of the movement of spherical rigid particles (equations (3.4) and (3.5)), is described by a set of Lagrangian points, uniformly distributed on the surface of each particle (see figure 3.1). The number of Lagrangian grid points, $N_L$, is selected to guarantee that the Lagrangian grid volume $\Delta V_l$ is as close as possible equal to the volume of the Eulerian mesh $\Delta x^3$. As mentioned before, the equations (3.1), (3.2), (3.4) and (3.5) are connected together with the ns/np boundary conditions on the surface of particle. A summary of the adopted numerical approach is given below:

- The Navier-Stokes equation (3.1) is integrated in time without the IBM force with the explicit low-storage three-step Runge-Kutta scheme (Spalart *et al.* 1991; Wesseling 2009) for all terms except the pressure gradient, i.e. for the viscous (in the inelastic fluids) and polymeric stress (in the visco-elatic fluids), where the Crank-Nicolson scheme is employed. The first prediction velocity $\mathbf{u}^*$ is calculated at each Runge-Kutta sub-step by:

  i) For generalised Newtonian fluids,

$$\begin{aligned}\mathbf{u}^* &= \mathbf{u}^{q-1} + \frac{\Delta t}{\rho_f}[-(\alpha_q+\beta_q)\nabla p^{q-3/2} - \rho_f\alpha_q(\nabla\cdot\mathbf{u}\otimes\mathbf{u})^{q-1} \\ &- \rho_f\beta_q(\nabla\cdot\mathbf{u}\otimes\mathbf{u})^{q-2} + \frac{(\alpha_q+\beta_q)}{2}(\nabla\cdot\boldsymbol{\tau})^q \\ &+ \frac{(\alpha_q+\beta_q)}{2}(\nabla\cdot\boldsymbol{\tau})^{q-1}]. \end{aligned} \tag{3.6}$$

  Where $\Delta t$ is the computational time step from $t^n$ to $t^{n+1}$, while the superscript $^q$ indicates the Runge-Kutta sub-step, with $q=0$ and $q=3$ corresponding to times $n$ and $n+1$. The Runge-Kutta constants can be found in e.g. Wesseling (2009): $\alpha_1 = 32/60$, $\beta_1 = 0$, $\alpha_2 = 25/60$, $\beta_2 = -17/60$, $\alpha_3 = 45/60$, $\beta_3 = -25/60$. It is noteworthy to mention that the viscosity of the inelastic fluids is obtained explicitly from the local shear-rate, using the velocities from the previous sub-step of the Runge-Kutta time integration scheme, and then $\boldsymbol{\tau}$ is computed from equation (2.1).

  ii) For visco-elastic fluids (Izbassarov *et al.* 2018),

$$\begin{aligned}\mathbf{u}^* &= \mathbf{u}^{q-1} + \frac{\Delta t}{\rho_f}[-(\alpha_q+\beta_q)\nabla p^{q-3/2} - \rho_f\alpha_q(\nabla\cdot\mathbf{u}\otimes\mathbf{u})^{q-1} \\ &- \rho_f\beta_q(\nabla\cdot\mathbf{u}\otimes\mathbf{u})^{q-2} + \frac{(\alpha_q+\beta_q)}{2}(\nabla\cdot\boldsymbol{\tau}_s+\nabla\cdot\boldsymbol{\tau}_m)^q \\ &+ \frac{(\alpha_q+\beta_q)}{2}(\nabla\cdot\boldsymbol{\tau}_s+\nabla\cdot\boldsymbol{\tau}_m)^{q-1}]. \end{aligned} \tag{3.7}$$

  A sufficient condition for a stable temporal integration is specified by the following criterion:

$$\Delta t \leq min\left(\frac{1.65}{12}\frac{\rho_f\Delta x^2}{(\mu_s+\mu_m)}, \frac{\sqrt{3}\Delta x}{\sum_{i=1}^{3}|u_i^q|}\right). \tag{3.8}$$

  Note that the spatial derivatives are computed with the second-order centered finite-difference scheme, except for the advection term $(\mathbf{u}\cdot\nabla\boldsymbol{\tau}_m)$ in equations (2.7) & (2.9), where the fifth-order weighted essentially non-oscillatory (WENO) scheme is adopted (Liu *et al.* 1994; Shu 2009;

Sugiyama *et al.* 2011; Rosti & Brandt 2017*a*; Shahmardi *et al.* 2019). Furthermore, to avoid the well-known numerical problems at high Weissenberg number for the Oldroyd-B and Giesekus fluid models, the log-conformation approach is applied to solve equations (2.7) & (2.9) (see section 3.2.2 for more details).

- The IBM force is calculated in three steps:

1) Interpolate $\mathbf{u}^*$ from the Eulerian grid to the Lagrangian points on the particle surface, $\mathbf{U}_l^*$ (equation 3.9a), employing the regularized Dirac delta function $\delta_d$ of Roma *et al.* (1999). This function is utilized to transfer between the two grids by interpolating the velocity and spreading the force through three adjacent Eulerian grid points (i.e. $3\Delta x$). Hence, it produces a smooth interface, effectively identical to a porous surface, which avoids high frequency oscillations of the force and torque on the particles and gives second-order accuracy in the velocity interpolation only if considering the effective diameter of the particle. The force and torque that fluid and particle exert onto each other , in the interpolation and spreading procedure, should be preserved. Therefore, the distribution of both Eulerian and Lagrangian grid points is equi-spaced with similar spacing.

2) compute the IBM force (per unit density) on the Lagrangian grid points, $\mathbf{F}_l^{q-1/2}$, based on the difference between the interpolated first prediction velocity and the particle velocity at those points (i.e. $\mathbf{U}_c^p + \boldsymbol{\omega}_c^p \times \mathbf{r}$).

3) Spread the IBM force from Lagrangian to the Eulerian grid points by the same regularized Dirac delta function (equation 3.9c). This IBM force, indicated as $\mathbf{f}_{ijk}^{q-1/2}$, is then added to the first prediction velocity to obtain a second prediction velocity $\mathbf{u}^{**}$ (equation 3.9d). In mathematical notation, these steps can be written as :

$$\mathbf{U}_l^* = \sum_{ijk} \mathbf{u}_{ijk}^* \delta_d \left( \mathbf{x}_{ijk} - \mathbf{X}_l^{q-1} \right) \Delta x \Delta y \Delta z \,, \tag{3.9a}$$

$$\mathbf{F}_l^{q-1/2} = \frac{\mathbf{U}^p \left( \mathbf{X}_l^{q-1} \right) - \mathbf{U}_l^*}{\Delta t} \,, \tag{3.9b}$$

$$\mathbf{f}_{ijk}^{q-1/2} = \sum_{l} \mathbf{F}_l^{q-1/2} \delta_d \left( \mathbf{x}_{ijk} - \mathbf{X}_l^{q-1} \right) \Delta V_l \,, \tag{3.9c}$$

$$\mathbf{u}^{**} = \mathbf{u}^* + \Delta t \mathbf{f}^{q-1/2} \,, \tag{3.9d}$$

where, in the above equations, the capital letters denote the variable at

a Lagrangian point with index $l$. $\mathbf{x}_{ijk}$ and $\mathbf{X}_l$ are the location of the Eulerian and Lagrangian grid points, respectively. An illustration of the Eulerian and Lagrangian grids used is presented in figure 3.1. Furthermore, to better enforce the boundary conditions at the moving surfaces, the IBM forces are iteratively computed by considering the multi-direct forcing scheme of Luo *et al.* (2007). The new second prediction velocity $\mathbf{u}^{**}$ is then found by solving the above equations iteratively (typically 3 iterations are sufficient) employing the new $\mathbf{u}^{**}$ as $\mathbf{u}^{*}$ at the beginning of the next iteration with equation 3.9b replaced by:

$$\mathbf{F}_l^{q-1/2} = \mathbf{F}_l^{q-1/2} + \frac{\mathbf{U}^p\left(\mathbf{X}_l^{q-1}\right) - \mathbf{U}_l^{**}}{\Delta t}\,. \tag{3.10}$$

- The second prediction velocity $\mathbf{u}^{**}$ is utilized to determine the correction pressure $\hat{p}$ and update the velocity for the next time step and the pressure field at the intermediate time step, $p^{q-1/2}$, following a classic pressure-correction scheme:

$$\nabla^2 \hat{p} = \frac{\rho_f}{(\alpha_q + \beta_q)\,\Delta t}\,\nabla\,.\,\mathbf{u}^{**}\,, \tag{3.11a}$$

$$\mathbf{u}^q = \mathbf{u}^{**} - \frac{(\alpha_q + \beta_q)\,\Delta t}{\rho_f}\,\nabla\hat{p}\,, \tag{3.11b}$$

$$p^{\,q-1/2} = p^{\,q-3/2} + \hat{p}\,, \tag{3.11c}$$

where $\mathbf{u}^q$ is the velocity at the Runge-Kutta sub-step $q$.

We take advantage of the simplicity of our geometry and boundary conditions (e.g., periodic in at least two directions), and the fact that we employ at least in two directions a regular, Cartesian grid, to solve the Poisson equation with a fast (FFT-based) direct approach (see for more details, Schumann & Sweet 1988).

Employing IBM and taking into account the the fictitious fluid phase inertia, enclosed within the particle volumes, equations (3.4) and (3.5) are rearranged as follows to maintain accuracy,

$$\rho_p V_p \frac{\mathrm{d}\mathbf{U}_c^p}{\mathrm{d}t} \approx -\rho_f \sum_{l=1}^{N_L} \mathbf{F}_l \Delta V_l + \rho_f \frac{\mathrm{d}}{\mathrm{d}t}\left(\int_{V_p} \mathbf{u}\mathrm{d}V\right) + (\rho_p - \rho_f)\,V_p \mathbf{g} + \mathbf{F}_c, \tag{3.12}$$

$$\mathbf{I}_p \frac{\mathrm{d}\boldsymbol{\omega}_c^p}{\mathrm{d}t} \approx -\rho_f \sum_{l=1}^{N_L} \mathbf{r}_l \times \mathbf{F}_l \Delta V_l + \rho_f \frac{\mathrm{d}}{\mathrm{d}t}\left(\int_{V_p} \mathbf{r} \times \mathbf{u}\mathrm{d}V\right) + \mathbf{T}_c\,, \tag{3.13}$$

where $\mathbf{r}_l$ indicates the distance between the center of a sphere and the $l-th$ Lagrangian points on its surface, while the second terms on the right-hand sides of equations (3.12) and (3.13) are corrections to account for the inertia of the fictitious fluid inside the sphere. This assists the numerical scheme to be more stable even for neutrally buoyant particles. These equations are advanced in time with the same Runge-Kutta method, introduced above, to compute $\mathbf{U}^p\left(\mathbf{X}_l^q\right)$ by (see Breugem (2012), for more details):

$$\mathbf{U}^p\left(\mathbf{X}_l^q\right) = \left(\mathbf{U}_c^p\right)^q + \left(\boldsymbol{\omega}_c^p\right)^q \times \mathbf{r}_l^q \,. \tag{3.14}$$

The force $\mathbf{F}_c$ and the torque $\mathbf{T}_c$ from equations (3.12) and (3.13) are employed to account for short-range hydrodynamic particle-particle and particle-walls interactions such as solid-solid contact or lubrication. These interactions are taken into account utilizing lubrication correction and the soft collision model as described in details in the work by Costa *et al.* (2015). When the gap distance between the particles and/or wall becomes less than one Eulerian mesh size, a mesh dependent lubrication correction based on asymptotic solution by Brenner (1961) is used to reproduce correctly the interaction between the particles. At very small gaps before the collision takes place, the lubrication correction is kept constant to account for the surface roughness. Additionally, a soft-sphere collision model is employed based on the relative velocity and the overlap between the two rigid spheres (spheres-wall) where both the normal and tangential contact force components are taken into account. The moment that the gap distance decreases to zero, i.e. collision takes place, the lubrication correction is switched off and the soft-sphere collision force model becomes active. The same models are employed for the interaction between particles and walls. Walls are implemented as spheres with infinite radius of curvature.

The volume fraction occupied by a rigid particle in an Eulerian grid cell with index $(i,j,k)$, used to compute the integrals above, $\varphi$, is computed by using the signed-distance level-set function $\varkappa$ suggested by Kempe & Fröhlich (2012), where $\varphi = 0$ and $\varphi = 1$ if a computational cell in the domain is located inside the fluid or in the solid phase. The sold volume fraction $\varphi$ is determined, at the pressure (cell center) and the velocity points (cell faces) throughout the staggered Eulerian grid, as follows:

$$\varphi_{i,j,k} = \frac{\sum_{n=1}^{8} -\varkappa_n \mathcal{H}(-\varkappa_n)}{\sum_{n=1}^{8} |\varkappa_n|} \,, \tag{3.15}$$

where $\mathcal{H}$ is the Heaviside step function with $\varkappa < 0$ inside and $\varkappa > 0$ outside the particle and the sum is over all 8 corners of a box of Eulerian cell around the target point.

The accuracy of the IBM code is investigated extensively among others in the work by Breugem (2012); Lambert *et al.* (2013); Costa *et al.* (2015); Picano *et al.* (2015). Also, the numerical code has been extensively validated for single and multiphase flows of visco-elastic and elastoviscoplastic fluids in

previous studies, and more details on the algorithm and validation campaign are described in previous references from the group (De Vita *et al.* 2018; Izbassarov *et al.* 2018; Shahmardi *et al.* 2019*b*), where very good agreement with literature results is obtained for various test cases.

### 3.2.2. *The log–conformation approach*

The numerical solutions of the visco-elastic constitutive equations, (2.7) & (2.9), are notoriously difficult especially in multi-phase flow systems mostly due to the large variation in time scales and discontinuous difference of visco-elastic properties through the interfaces (Izbassarov & Muradoglu 2015). In addition, many previous works revealed that the numerical solutions of these fluids are unstable, especially in the case of high Weissenberg numbers, because of the loss of resolution of discretization methods to solve the exponential growth of stresses at critical points over time (Pimenta & Alves 2017). A popular indicator of such unfavourable situation is the loss of positive definiteness of the conformation tensor (Fattal & Kupferman 2004), which can eventually lead to numerical breakdown. Various numerical approaches have been proposed to overcome these problems and most of them depend on a change of variable in the constitutive equation (Fattal & Kupferman 2004, 2005; Afonso *et al.* 2012; Balci *et al.* 2011). The log-conformation method, which can be applied to a wide variety of constitutive laws, suggested by Fattal & Kupferman (2004, 2005) became such a common methodology, This is based on the rewriting of the constitutive equation in terms of the logarithm of the conformation tensor, which surely remains positive definite and linearizes the polymer stress field in regions of exponential growth, hence increases the numerical stability even at high Weissenberg number (Afonso *et al.* 2009; Yang *et al.* 2016). In the current study, we follow basically this approach, which is briefly described next. For more details on the mathematics beyond each step, we refer the reader to the original works of Fattal & Kupferman (2004, 2005).

The relationship between the polymeric extra-stress tensor (for the Oldroyd-B or Giesekus model) and the conformation tensor, based on a model for the polymers as microscopic dumbbells with Hookean springs, is defined by (Bird *et al.* 1987):

$$\boldsymbol{\tau}_m = \frac{\mu_m}{\lambda_m}(\boldsymbol{C} - \boldsymbol{I}), \tag{3.16}$$

where $\boldsymbol{C}$ denotes the polymer conformation tensor scaled by the equilibrium Hookean spring length. $\boldsymbol{C}$ is defined as the pre-averaged dyadic product of the polymer end-to-end vector, $C_{ij} = \langle R_i R_j \rangle$, and is hence a symmetric tensor. In this method, equations (2.7) & (2.9) are written in terms of the conformation tensor $\boldsymbol{C}$, and the logarithm of the conformation tensor $\boldsymbol{\Psi} = log(\boldsymbol{C})$ is employed in the computations.The essential characteristic of this approach is the decomposition of the velocity gradient transpose $\nabla \mathbf{u}^T$ into two anti-symmetric tensors indicated by $\boldsymbol{\Omega}$ and $\boldsymbol{B}$, and a symmetric one specificed by $\boldsymbol{A}$ which

commutes with the conformation tensor, i.e.,

$$\nabla \mathbf{u}^T = \boldsymbol{\Omega} + \boldsymbol{A} + \boldsymbol{B}\boldsymbol{C}^{-1}. \tag{3.17}$$

The eventual formulation of the evolution equation in the variable $\boldsymbol{\Psi}$ can be written as (Yang *et al.* 2016),

$$\frac{\partial \boldsymbol{\Psi}}{\partial t} + \mathbf{u} \cdot \nabla \boldsymbol{\Psi} - (\boldsymbol{\Omega}\boldsymbol{\Psi} - \boldsymbol{\Psi}\boldsymbol{\Omega}) - 2\boldsymbol{A} = \boldsymbol{RHS}\,, \tag{3.18}$$

for the sake of simplicity, with $\boldsymbol{RHS} = \frac{1}{\lambda_m}(e^{-\boldsymbol{\Psi}} - \boldsymbol{I}) - \frac{\alpha}{\lambda_m} e^{-\boldsymbol{\Psi}}(e^{\boldsymbol{\Psi}} - \boldsymbol{I})^2$. Note that, when $\alpha = 0$, we recover the Oldroyd-B evolution equation.

This equation is integrated using the third-order Runge-Kutta scheme, introduced in section 3.2.1 (Izbassarov *et al.* 2018), i.e.,

$$\begin{aligned} \boldsymbol{\Psi}^q \;=\; & \boldsymbol{\Psi}^{q-1} + \Delta t\{\alpha_q \left[\boldsymbol{RHS} - (\mathbf{u} \cdot \nabla \boldsymbol{\Psi} - (\boldsymbol{\Omega}\boldsymbol{\Psi} - \boldsymbol{\Psi}\boldsymbol{\Omega}) - 2\boldsymbol{A})\right]^{q-1} \\ & - \beta_q \left[\boldsymbol{RHS} - (\mathbf{u} \cdot \nabla \boldsymbol{\Psi} - (\boldsymbol{\Omega}\boldsymbol{\Psi} - \boldsymbol{\Psi}\boldsymbol{\Omega}) - 2\boldsymbol{A})\right]^{q-2}\}\,. \end{aligned} \tag{3.19}$$

$\boldsymbol{\Psi}$ is then converted back to the conformation tensor, $\boldsymbol{C} = e^{\boldsymbol{\Psi}}$, to compute the polymer stress $\boldsymbol{\tau_m}$ by using equation (3.16), hence solving equation (3.7) to calculate the first prediction velocity $\mathbf{u}^*$. It is worth noting that, the conformation tensor $\boldsymbol{C}$ is imposed to be $\mathbf{I}$ inside the spheres via a smooth phase indicator that points to 1 in the fluid phase and gradually varies to 0 within a gap (gap normal to the surface) of $1.5\Delta x$ inside the spheres. Moreover, equation (3.18) is discretized around the Eulerian cell centers (pressure points on the Eulerian staggered grid) and the spatial derivatives are again approximated with the second-order central-difference scheme, except for the advection terms $(\mathbf{u} \cdot \nabla \boldsymbol{\Psi})$, where the fifth-order WENO scheme is used. WENO schemes are non-linear finite-volume or finite-difference approaches which can numerically estimate solutions of hyperbolic conservation laws and other convection controlled problems with high-order accuracy in smooth zones and substantially non-oscillatory transition for solution discontinuities (Rosti *et al.* 2019*b*).

## 3.3. Volume penalization IBM

The immersed boundary method can also be used to create a virtual pipe geometry in the computational domain. In current study we have employed the Volume penalization IBM to create a virtual circular straight pipe from a simple square duct domain with a staggered Cartesian grid, by enforcing the no-slip and no-penetration boundary conditions on the inner surface of the pipe. This method has been proposed by Kajishima *et al.* (2001); Breugem *et al.* (2014), where the IBM force $\mathbf{f}$ and the second prediction velocity $\mathbf{u}^{**}$ are determined as follows:

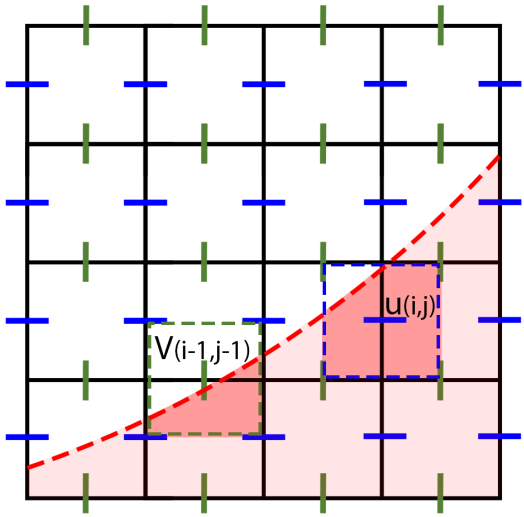


Figure 3.2: Solid volume fractions (highlighted area) for mesh cells around $u(i,j)$ and $v(i-1,j-1)$. Solid boundary is shown by red dashed line; figure from (Izbassarov *et al.* 2018).

$$\mathbf{f}_{ijk} = \varphi_{i,j,k} \frac{(\mathbf{u}^s - \mathbf{u}^*)_{ijk}}{\Delta t}\,, \tag{3.20a}$$

$$\mathbf{u}^{**}_{ijk} = \mathbf{u}^{*}_{ijk} + \Delta t \mathbf{f}_{ijk}\,, \tag{3.20b}$$

where, the solid volume fraction in the mesh cells $\varphi_{i,j,k}$ is also varied between 1 (wholly located in the fluid phase) and 0 (wholly located in the solid domain) and $\mathbf{u}^s$ indicates the solid interface velocity within this mesh cell. Figure 3.2 displays the solid volume fractions (highlighted area) for mesh cells around $u(i,j)$ and $v(i-1,j-1)$. In this figure, the solid boundary is indicated by the red dashed line. For stationary boundaries, $\mathbf{u}_s$ is 0 and equations 3.20 reduce to:

$$\mathbf{u}^{**}_{ijk} = (1 - \varphi_{i,j,k})\, \mathbf{u}^{*}_{ijk}\,. \tag{3.21}$$

The second prediction velocity $\mathbf{u}^{**}$ is then employed to update velocities and pressure following the steps described previously in equations 3.11.

From a numerical point of view, the volume penalization IBM is very efficient, since the solid volume fractions around velocity points can be computed at the beginning of the simulation with an accurate approach or it can be found from different methods such as magnetic resonance imaging and X-ray computed tomography in case of a complex geometry or flow through porous media

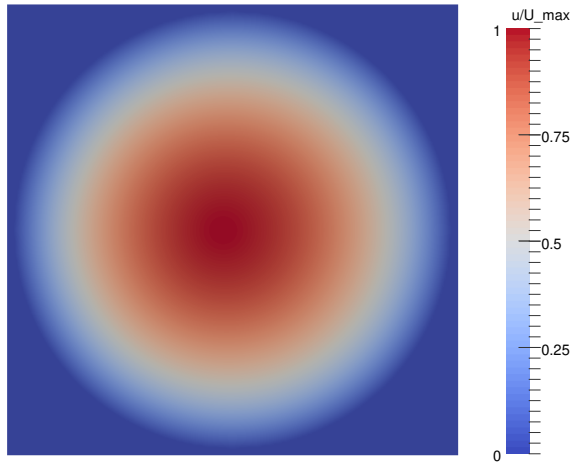


Figure 3.3: Contours of streamwise velocity in the circular cross section of a pipe at $Re = 400$, simulated by volume penalization IBM.

(Breugem *et al.* 2014). Figure 3.3 displays an example of how the square duct with a staggered cartesian grid is converted into a pipe via a volume penalization technique.

Chapter 4

# Deformable hyper-elastic particles in a flow

In this chapter, we briefly describe the governing equations for the motion of a single deformable viscous hyper-elastic particle suspended in a Newtonian fluid flow and the numerical method used to solve them. Hyper-elastic materials reveal non-linear stress-strain curves and are generally employed to describe gel- and rubber-like materials; for example, Verma & Kumaran (2013) obtained a good agreement between experimental and numerical results if a soft gel is modelled as an incompressible viscous hyper-elastic material such as the one used here.

## 4.1. Governing equations

We consider a deformable viscous hyper-elastic particle immerse in a Newtonian viscous fluid, both the fluid and solid phases are incompressible and their motion is governed by the conservation of momentum and the incompressibility constraint:

$$\rho\left(\frac{\partial \mathbf{u}^{\mathrm{f}}}{\partial t}+\mathbf{u}^{\mathrm{f}}\cdot\nabla\mathbf{u}^{\mathrm{f}}\right)=\nabla\cdot\boldsymbol{\sigma}^{\mathrm{f}}, \tag{4.1a}$$

$$\nabla\cdot\mathbf{u}^{\mathrm{f}}=0, \tag{4.1b}$$

$$\rho\left(\frac{\partial \mathbf{u}^{\mathrm{s}}}{\partial t}+\mathbf{u}^{\mathrm{s}}\cdot\nabla\mathbf{u}^{\mathrm{s}}\right)=\nabla\cdot\boldsymbol{\sigma}^{\mathrm{s}}, \tag{4.1c}$$

$$\nabla\cdot\mathbf{u}^{\mathrm{s}}=0, \tag{4.1d}$$

where the superscripts $^{\mathrm{f}}$ and $^{\mathrm{s}}$ in the previous equations are utilized to distinguish the fluid and solid phases, and $\rho$ is the density, assumed to be the same in both phases. The kinematic and dynamic interactions between the two phases are found by forcing the continuity of the velocity (i.e., the no-slip and no-penetration boundary conditions) and of the traction force (i.e., a traction balance) at the interface, i.e.,

$$\mathbf{u}^{\mathrm{f}}=\mathbf{u}^{\mathrm{s}}, \tag{4.2a}$$

$$\boldsymbol{\sigma}^{\mathrm{f}}\mathbf{n}=\boldsymbol{\sigma}^{\mathrm{s}}\mathbf{n}, \tag{4.2b}$$

where $\mathbf{n}$ indicates the normal vector at the interface.The Cauchy stress tensor $\boldsymbol{\sigma}$ for a Newtonian fluid and for an incompressible viscous hyper-elastic material experiencing only the isochoric motion, i.e. the motion that preserves the volume of every part of the material body, can be written as:

$$\boldsymbol{\sigma}^{\mathrm{f}} = -P\mathbf{I} + 2\mu^{\mathrm{f}}\boldsymbol{\Theta}^{\mathrm{f}}\,, \tag{4.3}$$

$$\boldsymbol{\sigma}^{\mathrm{s}} = -P\mathbf{I} + 2\mu^{\mathrm{s}}\boldsymbol{\Theta}^{\mathrm{s}} + G\boldsymbol{\xi}\,, \tag{4.4}$$

where $\mu^{\mathrm{f}}$ and $\mu^{\mathrm{s}}$ represent the dynamic viscosity of the fluid and solid phases, respectively. The last term, $G\boldsymbol{\xi}$, is the hyper-elastic stress contribution modeled as a neo-Hookean material, satisfying the incompressible Mooney-Rivlin law, where $G$ denotes the modulus of transverse elasticity and $\boldsymbol{\xi}$ is the deviatoric left Cauchy-Green deformation tensor (also sometimes called Finger deformation tensor). The tensor $\boldsymbol{\xi}$ is updated by the following transport equation:

$$\frac{\partial\boldsymbol{\xi}}{\partial t} + (\mathbf{u}\cdot\nabla)\,\boldsymbol{\xi} - \boldsymbol{\xi}\cdot\nabla\mathbf{u} - \nabla\mathbf{u}^{T}\cdot\boldsymbol{\xi} = 0\,, \tag{4.5}$$

where $\boldsymbol{\xi}\cdot\nabla\mathbf{u} + \nabla\mathbf{u}^{T}\cdot\boldsymbol{\xi}$ describes the stretching of the elastic material due to the straining action of the flow. This equation comes from the fact that the upper convected derivative of the tensor $\boldsymbol{\xi}$ is identically zero, which is always true for an hyper-elastic material (Bonet & Wood 1997).

## 4.2. Numerical method

To numerically solve the fluid-structure interaction at the interface, the so called one-continuum formulation (Tryggvason *et al.* 2007) is considered, where only one set of equations is solved over the whole field. This is obtained by introducing a monolithic velocity vector field, $\mathbf{u}$, valid everywhere; this is the weighted average between the values in the two phases, with the weight being a phase indicator function $\psi$ based on the local solid volumetric fraction in each cell (Quintard & Whitaker 1994; Takeuchi *et al.* 2010)

$$\mathbf{u} = (1-\psi)\,\mathbf{u}^{\mathrm{f}} + \psi\mathbf{u}^{s}. \tag{4.6}$$

Thus, $\psi$ changes smoothly from 0 in the fluid phase to 1 in the solid phase. In particular, the isoline at $\psi = 0.5$ represents the interface (see figure 4.1). The scalar $\psi$ is computed by solving an additional transport equation

$$\frac{\partial\psi}{\partial t} + \mathbf{u}\cdot\nabla\psi = 0\,. \tag{4.7}$$

Hence, the governing equations (4.1) can be rewritten as:

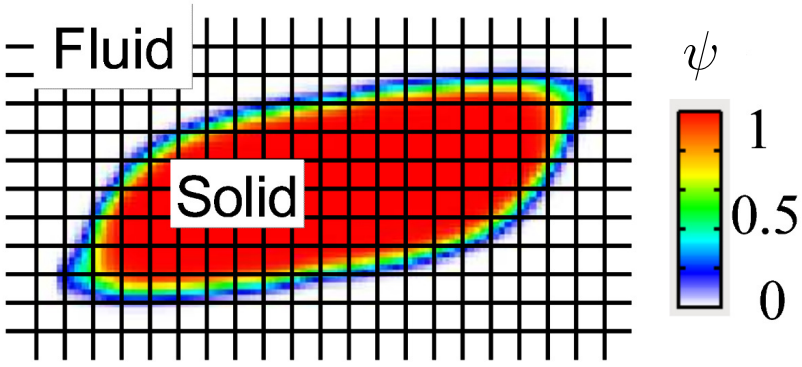


Figure 4.1: Skech of the 2D Eulerian grids used in the one-continuum formulation approach. The different values of the solid volume fraction $\psi$ are represented by different colors. The contour at $\psi = 0.5$ denotes the interface; figure from (Sugiyama *et al.* 2011).

$$\rho\left(\frac{\partial \mathbf{u}}{\partial t} + \mathbf{u}\cdot\nabla\mathbf{u}\right) = \nabla\cdot\boldsymbol{\sigma}, \tag{4.8a}$$

$$\nabla\cdot\mathbf{u} = 0, \tag{4.8b}$$

where the Cauchy stress tensor $\boldsymbol{\sigma}$ is written in a mixture form and defined as

$$\boldsymbol{\sigma} = (1-\psi)\,\boldsymbol{\sigma}^f + \psi\boldsymbol{\sigma}^s. \tag{4.9}$$

The equations (4.7), (4.8) and (4.5) are solved in a fully Eulerian formulation on a staggered uniform mesh with velocities located on the cell faces and all the other variables (pressure, fluid and solid stress components) at the cell centers, as first proposed by Sugiyama *et al.* (2011). The time integration is based on an explicit fractional-step method (Kim & Moin 1985), where only the solid hyper-elastic contribution in equation (4.1) is advanced with the Crank-Nicolson scheme (Min *et al.* 2001), while, all the other terms are advanced with the third order Runge-Kutta scheme, introduced in chapter 3 . All the spatial derivatives are approximated with the second-order centred finite differences scheme, except for the advection term in equations (4.5) and (4.7) where the fifth-order WENO scheme is applied (Shu 2009; Sugiyama *et al.* 2011; Shahmardi *et al.* 2019). A comprehensive review on the effect of different discretization schemes for the

advection terms was studied by Min *et al.* (2001). The pressure is computed by solving the Poisson equation using fast Fourier transforms. In summary, the set of governing equations are solved as follows (see Rosti & Brandt 2017): (i) the left Cauchy-Green deformation tensor $\xi_{ij}$ and the local solid volume fraction $\psi$ are updated first by solving Equations 4.5 and 4.7 (update step); (ii) the conservation of momentum equation 4.8 are advanced in time by first solving the momentum equation (prediction step), then by solving a Poisson equation for the projection variable and finally by correcting the pressure and velocity to ensure that the velocity field is divergence free (correction step).

The accuracy and validity of the code has been extensively examined in previous studies, and more details on the numerical scheme and validation campaign are shown in Refs. (see Rosti & Brandt 2017, 2018; Rosti *et al.* 2018), where very good agreement with literature results is found for different test cases. In addition, for more details on the numerical method, the reader is referred to Ref. Sugiyama *et al.* (2011).

Chapter 5

# Summary of the papers

## Paper 1

*Interface-resolved simulations of particle suspensions in Newtonian, shear thinning and shear thickening carrier fluids*

We present a numerical study of noncolloidal spherical and rigid particles suspended in Newtonian, shear thinning and shear thickening fluids employing an Immersed Boundary Method. We consider a linear Couette configuration to explore a wide range of solid volume fractions ($0.1 \leq \Phi \leq 0.4$) and particle Reynolds Numbers ($0.1 \leq Re_p \leq 10$).

We report the distribution of solid and fluid phase velocity and solid volume fraction and show that close to the boundaries inertial effects result in a significant slip velocity between the solid and fluid phase. The local solid volume fraction profiles indicate particle layering close to the walls, which increases with the nominal $\Phi$. This feature is associated with the confinement effects.

We calculate the probability density function of local strain rates and compare their mean value with the values estimated from the homogenization theory of Chateau *et al.* (2008), indicating a reasonable agreement in the Stokesian regimes. Both the mean value and standard deviation of the local strain rates increase primarily with the solid volume fraction and secondarily with the $Re_p$. The wide spectrum of the local shear rate and its dependency on $\Phi$ and $Re_p$ points to the deficiencies of the mean value of the local shear rates in estimating the rheology of these noncolloidal complex suspensions.

Finally, we show that in the presence of inertia, the effective viscosity of these noncolloidal suspensions deviates from that of Stokesian suspensions. We discuss how inertia affects the microstructure and provide a scaling argument to give a closure for the suspension shear stress for both Newtonian and power-law suspending fluids. The stress closure is valid for moderate particle Reynolds numbers, $O(Re_p) \sim 10$.

## Paper 2

*Interface-resolved simulations of particle suspensions in visco-elastic carrier fluids*

We study the rheology of a suspension of neutrally buoyant rigid particles subject to uniform shear in different kinds of non-Newtonian fluids, chosen in order to disentangle the effect of elasticity and shear thinning on the macroscopic system behavior. In particular, we adopt the inelastic Carreau, viscoelastic Oldroyd-B and Giesekus models for the carrier fluid. The rheology of the suspension is analyzed for a wide range of particle volume fractions ($0.1 \leq \Phi \leq 0.4$), Weissenberg ($0.1 \leq Wi \leq 3$) and Reynolds numbers ($0.5 \leq Re_p \leq 15$), comparing the results with those obtained for a Newtonian carrier fluid.

We report here that the effective viscosity pertaining all the non-Newtonian cases is always lower than that of the suspension in the Newtonian carrier fluid and grows monotonically with the solid volume fraction. The shear-thinning viscoelastic Giesekus fluid behaves similarly to the Oldroyd-B fluid at low Weissenberg numbers and to the Carreau fluid at high Weissenberg numbers, indicating that elastic effects dominate at low Weissenberg and shear thinning is predominant at high Weissenberg number. These variations in the effective viscosity are mainly due to changes in the particle induced shear stress component. These data show that, at high shear rates, a viscoelastic carrier fluid can be modelled as a simple shear-thinning fluid for which theoretical closures exists, while new models are needed at low Weissenberg numbers to account for elastic effects such as decreased particle stress.

Finally, when the inertia is increased, the suspension effective viscosity grows with the particle Reynolds number at the same rate as in a Newtonian fluid for the Oldroyd-B case, while in a shear-thinning fluid the growth is less than in the Newtonian fluid. Also in the presence of inertia, therefore, the shear-thinning behavior dominates the suspension dynamics at relatively high values of the imposed shear rate and elasticity effects saturate.

**Paper 3**

*Sedimentation of finite-size particles in quiescent wall-bounded shear-thinning and Newtonian fluids*

We study the sedimentation of finite-size particles in quiescent wall-bounded Newtonian and shear-thinning fluids. The problem is studied numerically by means of direct numerical simulations with the presence of the particles accounted for with an immersed boundary method. The suspended phase consists of Non-Brownian rigid spherical particles with particle to fluid density ratio $\rho_p/\rho_f = 1.5$; three different solid volume fractions $\Phi = 1\%$, $5\%$ and $20\%$ are considered. The Archimedes number is kept constant to $Ar = 36$ for all shear-thinning fluids, while it is changed to $Ar = 97$ for the Newtonian fluid

to reproduce the same terminal velocity of a single particle sedimenting in the shear-thinning fluid.

We show that the mean settling velocities decrease with the particle concentration as a consequence of the hindering effect and that the mean settling speed is always larger in the shear thinning fluid than in the Newtonian one. This is due to the decrease of the mean viscosity of the fluid which leads to a lower drag force acting on the particles. We show that particles tend to form aggregates in the middle of the channel in a shear-thinning fluid, preferentially positioning in the wake of neighboring particles or aside them, resulting in lower levels of fluid velocity fluctuation in the gravity direction than in a Newtonian fluid.

### Paper 4

*Inertial migration of a deformable particle in pipe flow*

We perform fully Eulerian numerical simulations of an initially spherical hyperelastic particle suspended in a Newtonian pressure-driven flow in a cylindrical straight pipe. We study the full particle migration and deformation for different Reynolds numbers and for various levels of particle elasticity, to disentangle the interplay of inertia and elasticity on the particle focusing.

We observe that the particle deforms and undergoes a lateral displacement while traveling downstream through the pipe, finally focusing at the pipe centerline. We note that the migration dynamics and the final equilibrium position are almost independent of the Reynolds number, while they strongly depend on the particle elasticity; in particular, the migration is faster as the elasticity increases (i.e. the particle is more deformable), with the particle reaching the final equilibrium position at the centerline in shorter times.

Our simulations show that the results are not affected by the particle initial conditions, position and velocity. Finally, we explain the particle migration by computing the total force acting on the particle and its different components, viscous and elastic.

Chapter 6

# Conclusions and outlook

During the years of this thesis work, we have examined suspensions of finite-size rigid spherical particles in simple canonical wall-bounded flow configurations (e.g., simple shear Couette flow for rheological studies and falling of particles by the action of gravity in a narrow channel) considering different kinds of Newtonian and Non-Newtonian fluids, trying to cover a wide range of parameters. Indeed, many parameters define a particle suspensions, such as particle size and density, volume fraction, as well as flow parameters like Reynolds number and fluid relative elasticity, the Weissenberg number. As concerns the non-Newtonian properties of the flow, we have employed both inelastic (Carreau and power-law), and visco-elastic models (Oldroyd-B and Giesekus) to examine separately the shear-thinning, shear-thickening, elasticity and combined shear-thinning visco-elastic features of the most commonly encountered non-Newtonian fluids. Particle-resolved direct numerical simulations have been performed using an immersed boundary method for the fluid-solid interactions to investigate the interaction between particles and fluid in the different flow cases. In addition, we have investigated the case of an hyper-elastic neo-Hookean deformable particle suspended in a Newtonian pressure-driven flows in a cylindrical straight pipe. A fully Eulerian numerical algorithm based on the one-continuum formulation is employed to fully resolve the fluid-structure interactions and the stresses in the liquid and solid phases and to provide an accurate understanding of the mutual effects of inertia and particle elasticity on the motion of a single deformable particle in a pipe flow. To this end, we have implemented a volume penalization IBM, creating virtual walls to simulate a circular pipe flow within a cartesian implementation with computational efficiency.

Several results are obtained from these simulations; the main conclusions that have drawn and the suggestions for possible future studies in each subject are summarized below.

## 6.1. Concluding remarks

### Suspension of rigid spheres in Newtonian and Non-Newtonian fluids in wall-bounded Couette flows

The study of the rheology of particle suspensions in Newtonian and non-Newtonian media is essential in a large number of industrial and biological applications and environmental processes. Among of these we recall concrete casting, pastes, paints, crude oil flows with rocks, particulate foods processing, waste disposal, drilling muds, slurry flows, pharmaceutical processes, the blood flow in the human body, pyroclastic flows from volcanoes and debris flows. Therefore, we have studied suspensions of neutrally buoyant spheres in both Newtonian and inelastic non-Newtonian fluids. We have explored four solid volume fractions, $\Phi = [0.11, 0.21, 0.315, 0.4]$, from very dilute to semi-dense, and a wide range of particle Reynolds numbers ($0 < Re_p \leq 10$) to examine also the role of inertia. We have initially considered inelastic non-Newtonian fluids and compared our results with the recently proposed constitutive laws based on the homogenisation theory (see Chateau *et al.* 2008), aiming to test the validity and possibly extend these laws for the cases when inertia is present. We have demonstrate that the non-dimensional relative viscosity of suspensions in Carreau shear-thinning and power-law shear-thickening carrier fluids can be well predicted by the homogenization theory of Chateau *et al.* (2008) in the limit of $Re_p \to 0$, and more accurately for lower $\Phi$. At higher volume fractions, the shear rates can locally become very large, so that predictions based on mean values become inaccurate, masking the breadth of the shear-rate distributions and the role of rare strong events.

In addition, we have shown that adding inertia to the system changes the microstructure and results in a deviation of the relative viscosity of the suspensions from the Stokesian prediction, while the main dissipation mechanism is still viscous. In fact, we have shown that for the parameter range explored here both particle stresses and fluid stresses are clustered about viscous scalings. We have therefore adopted the frictional view of Cassar *et al.* (2005); Andreotti *et al.* (2013) to show that the main dimensionless number controlling the mechanics of suspensions is the so-called viscous number, $J \sim \mu_f(\bar{\dot{\gamma}}_{local})\dot{\gamma}/P$, confirming that viscous stresses are responsible for the momentum transport even when the particle Reynolds number is finite. However, due to inertial effects, the microstructure becomes anisotropic and so-called shadow regions form around particles (these are regions with zero probability of finding another particle, see Picano *et al.* 2013). This enhances the effective particle volume fraction, and consequently, the viscous dissipation and relative viscosity. We have estimated the volume of these shadow regions from our simulations and included this microstructural effect into a functional form for the relative viscosity. In this way, we have provided a prediction for the added excluded volume due to inertia and a closure for the suspension stress in the case of both Newtonian and generalized Newtonian suspending fluids valid for $O(Re_p) \sim 10$ (see paper 1).

Motivated by other typical effects present in non-Newtonian fluids, we have also examined the role of fluid elasticity and shear thinning and of the combination of shear-thinning and visco-elastic effects on the simple shear flow of neutrally-buoyant rigid spherical particles in suspension. To this end, we have

used different models for the carrier fluid (Oldroyd-B, Carreau and Giesekus for purely elastic, shear-thinning and a possibly more realistic shear-thinning visco-elastic polymer suspension). We have analyzed the rheology of the suspension by discussing how the suspension effective viscosity $\mu_{eff}$ is affected by variations of the particle volume fraction $\Phi$, the Weissenberg number $Wi$ and the particle Reynolds number $Re_p$ for all the different fluids, comparing the results with those obtained for a Newtonian carrier fluid. We have observed that, at low level of inertia, the effective viscosity for all fluids considered grows monotonically with the solid volume fraction $\Phi$ and that all the Non-Newtonian cases exhibit a lower effective viscosity than the Newtonian ones. In particular, we have found that the shear-thinning fluid has the highest effective viscosity among the Non-Newtonian fluids, while the Oldroyd-B fluid has the lowest values. The effective viscosity is only slightly dependent on the Weissenberg number $Wi$: at low Weissenberg number the shear thinning effect is weak and the Carreau fluid exhibits a high effective viscosity $\mu_{eff}$ close to the value found in a Newtonian fluid; on the other hand, the elastic effects in the Giesekus and Oldroyd-B fluids are always present even at low $Wi$. We have observed that the Giesekus fluid behaves similarly to the Oldroyd-B one at low $Wi$ when the elasticity dominates, while it behaves similarly to the Carreau fluid at high $Wi$ when the shear thinning effect is predominant. When inertia is considered, but still limited to low values where the total stress are viscosity dominated, the suspension effective viscosity grows with the particle Reynolds number. The Oldroyd-B fluid exhibit a very similar behavior to the Newtonian carrier fluid, with $\mu_{eff}$ growing at the same rate. The shear thinning fluid instead grows less than the Newtonian fluid and thus effectively reduces the inertial shear thickening of the suspension. The Giesekus fluid shows an effective viscosity similar to the Oldroyd-B one at low $Re_p$ when elasticity dominates over the shear thinning and to the Carreau one at high $Re_p$ when the shear thinning becomes predominant (see paper 2), which again confirms that at high shear rates or high $Weissenberg$ numbers, the shear-thinning behavior dominates also in suspensions.

**Sedimentation**

The gravity-driven motion of finite-size heavy particles in a viscous fluid is relevant in many environmental, biological and industrial applications, yet this has mainly been investigated for sedimentation of spherical particles in Newtonian fluid. We have therefore investigated numerically the effect of a shear-thinning fluid on the settling behavior of monodisperse rigid sphere suspensions in a quiescent wall-bounded environment with fixed ratio between the particle diameter and channel width equal to 1/18, particle to fluid density ratio $\rho_p/\rho_f = 1.5$ for three different solid volume fractions, $\Phi = [0.01, 0.05, 0.2]$, and compared the results with those obtained in a Newtonian fluid. The Archimedes number is set to $Ar = 36$ for all non-Newtonian fluid cases while it is increased to $Ar = 97$ for the Newtonian ones to obtain almost the same

value of the settling velocity of an isolated particle (same terminal Reynolds number $Re_t = 3.89$) as in the shear-thinning case. In particular, we have examined the mean particle settling and fluid velocities, the standard deviation of the different velocities, wall effects and microstructure of these complex suspensions. We have found that the mean settling velocity of a suspension decreases with $\Phi$ and increase in the shear-thinning fluid. This is the result of the competition between two opposite effects, related to different physical mechanisms: i) the hindrance effect, which reduces the mean settling velocity and monotonically increases with $\Phi$; ii) the shear-thinning effect, which also increases with $\Phi$ as a consequence of the reduction of the local fluid viscosity around the particles and leads to an increase of the mean settling velocity. By analysing the probability density function of the settling velocity, we have reported a high probability of particles settling faster than the mean settling velocity at low concentrations, while the opposite trend has been found for high volume fractions. This effect is present in both fluids, but it is strengthened in the shear-thinning fluid. We have also found a large value of the fourth-order moment in the non-Newtonian fluid, indicating a highly intermittent behavior at low volume fractions, which eventually vanishes at higher concentrations. At low volume fraction, we have shown that intrinsic convection occurs through the channel in both carrier fluids, which induces an increase of the particles settling velocity in the channel center. Interestingly, this convection is reversed at the highest volume fraction investigated, especially in the Newtonian fluid. We have also revealed the tendency to form aggregates in a shear-thinning fluid, with particles preferentially positioning in the wake or beside each other, which overall results in lower levels of velocity fluctuations in the gravity direction than in a Newtonian fluid (see paper 3).

**Deformable particle in pipe flow**

We have studied the motion of an hyper-elastic deformable particle immersed in a Newtonian Poiseuille flow in a cylindrical straight pipe at different finite Reynolds and Weber numbers, in order to evaluate the effects of inertia and elasticity on the particle focusing. We have focused on the lateral motion of the particle and compared the entire migration dynamics, the trajectory, and the final equilibrium shape of the particle to shed more light onto the particle lateral displacement mechanism. We have shown that the particle deforms and undergoes a lateral displacement while traveling downstream through the pipe, always focusing at the pipe centerline. While the particle final equilibrium position is independent of the Reynolds and Weber numbers considered, its migration dynamics strongly depends on the particle elasticity while it is only slightly affected by the Reynolds number. In particular, the migration is faster as the elasticity increases, with the particle reaching the final equilibrium position at the centerline in shorter times when more deformable. We also have shown the effect of the solid to fluid viscosity ratio and observed that high solid viscosity makes the particle effectively more rigid, so that it requires a longer

time to reach the equilibrium position when compared to cases with low values of solid viscosity (see paper 4).

## 6.2. Outlook

In future, we would like to expand our knowledge in the field of particle suspensions in non-Newtonian fluids. Concerning the suspension in simple shear flows, this work provides new insights on the rheology of suspensions of rigid objects in Non-Newtonian fluids, and proves the existence of a variety of non-trivial effects brought by the coupling of shear-thickening particulate suspensions and non-Newtonian fluids. This work can be extended in a number of ways, where additional simulations and experiments are needed to provide new closures for particle-laden suspensions in non-Newtonian matrices. Also, the effect of particles with different shapes, such as oblate or biconcave red-blood cells, should be considered, especially for analysis in confined geometries. In addition, it would be interesting to consider slightly more complex configurations, such as oscillating shear and separating flows, to gain a better understanding on the interactions between a time-dependent flow, the fluid memory and the modifications of the particle microstructure.

Regarding the sedimentation of particles in quiescent wall-bounded fluid, with this investigation we have estimated the effect of a shear-thinning fluid on the sedimentation of a suspension of inertial particles. Future works should extend the analysis to more complex non-Newtonian fluids, taking into account, for example, the role of elasticity and yield stress. In addition, it will be interesting to explore more in detail the parameter space defined by the particle shape, Archimedes number and density ratio. To this end, experiments may appear as a viable tool, given the cost of interface-resolved numerical simulations.

In the context of the inertial migration of deformable particles in pipe flows, these results provide useful knowledge for the design of a microfluidic cylindrical system at finite inertia e.g. for flow focusing of deformable particles and flow sorting based on particle elasticity $G$. In particular, for the design of devices of high throughput, it would be important to consider suspensions of deformable particles in dilute conditions as well as the effect of the presence of smaller rigid particles in the flow, both in cylindrical pipes and square ducts, as it is the case in several biomedical applications. The interaction between the particle and fluid elasticity, i.e. the case of a viscoelastic suspending fluid, might also provide useful suggestions for the design of microfluidic systems.

# Acknowledgements

First and foremost, I would like to thank my main supervisor, Prof. Luca Brandt, for giving me the opportunity to come to KTH and work under his guidance on this research project. I am deeply grateful for your trust, patience, dedication and inspiring advices over the last five years. This thesis would not exist if it hadn't been for your continued support and resilience. Luca, *grazie mille!* Also many thanks to Dr. Minh Do-Quang as my co-advisor.

Next, I would like to thank Dr. Sarah Hormozi for sharing her knowledge while working together. Many thanks to my colleagues and co-authors, Iman, Marco and Walter, who contributed a lot to this thesis. Special thanks to my incredible friends Mehdi and Daulet for sharing their knowledge and experiences with me to improve my numerical skills. I am also grateful to Niclas Berg for the Swedish abstract. Special thanks also to Prof. Lisa Prahl Wittberg for reviewing this thesis and sharing her valuable feedback.

I am grateful to my many friends and colleagues at the department, past and present, for creating such a friendly atmosphere. I wish to first thank my nice officemates Velibor, Nicolò and Matteo and at this point of my research experience at KTH, I would say to you, *guys, I will do like Baglioni!* I wish to thank other people in the department including the ones who were here befor; Ali, Armin, Arash, Omid, Anthony, Pedro, Nima, Kazem, Azad, Emad, Song, Giandomenico, Jacopo, Prabal, Francesco, Sagar, Hamid, Shyang Maw, Elektra, Mattias, Clio, Nicolas and Ugis. I would thank administrative and technical staff in the department, Heide, Viviana, Stefan and human resource managers for all the preparations.

*Last but not least, I would like to express my sincere gratitude to my wife Fatimaalzhra for her love, patience and understanding, to my parents and brothers for their unconditional support and trust, to my kids Jannat, Baqer, Fajr and Revan for all their endless love.*

# Bibliography


Afonso, A., Oliveira, P. J., Pinho, F. & Alves, M. 2009 The log-conformation tensor approach in the finite-volume method framework. *Journal of Non-Newtonian Fluid Mechanics* **157** (1-2), 55–65.

Afonso, A., Pinho, F. & Alves, M. 2012 The kernel-conformation constitutive laws. *Journal of Non-Newtonian Fluid Mechanics* **167**, 30–37.

Alghalibi, D., Lashgari, I., Brandt, L. & Hormozi, S. 2018*a* Interface-resolved simulations of particle suspensions in newtonian, shear thinning and shear thickening carrier fluids. *Journal of Fluid Mechanics* **852**, 329–357.

Alghalibi, D., Lashgari, I., Brandt, L. & Hormozi, S. 2018*b* Interface-resolved simulations of particle suspensions in newtonian, shear thinning and shear thickening carrier fluids. *Journal of Fluid Mechanics* **852**, 329–357.

Allen, E. & Uhlherr, P. 1989 Nonhomogeneous sedimentation in viscoelastic fluids. *Journal of Rheology* **33** (4), 627–638.

Amarsid, L., Delenne, J.-Y., Mutabaruka, P., Monerie, Y., Perales, F. & Radjai, F. 2017 Viscoinertial regime of immersed granular flows. *Physical Review E* **96** (1), 012901.

Amini, H., Lee, W. & Di Carlo, D. 2014 Inertial microfluidic physics. *Lab on a Chip* **14** (15), 2739–2761.

Andreotti, B., Forterre, Y. & Pouliquen, O. 2013 *Granular media: between fluid and solid*. Cambridge University Press.

Ardekani, M. N., Costa, P., Breugem, W. P. & Brandt, L. 2016 Numerical study of the sedimentation of spheroidal particles. *International Journal of Multiphase Flow* **87**, 16–34.

Asmolov, E. S. 1999 The inertial lift on a spherical particle in a plane poiseuille flow at large channel reynolds number. *Journal of Fluid Mechanics* **381**, 63–87.

Ateya, D. A., Erickson, J. S., Howell, P. B., Hilliard, L. R., Golden, J. P. & Ligler, F. S. 2008 The good, the bad, and the tiny: a review of microflow cytometry. *Analytical and bioanalytical chemistry* **391** (5), 1485–1498.

Bächer, C., Schrack, L. & Gekle, S. 2017 Clustering of microscopic particles in constricted blood flow. *Physical Review Fluids* **2** (1), 013102.

Bagchi, P. 2007 Mesoscale simulation of blood flow in small vessels. *Biophysical journal* **92** (6), 1858–1877.

Bagnold, R. 1954 Experiments on a gravity-free dispersion of large solid spheres in a Newtonian fluid under shear. *Proc. Royal Soc. London. Series A. Math. and Phys. Sci.* **225**, 49–63.

Balci, N., Thomases, B., Renardy, M. & Doering, C. R. 2011 Symmetric

factorization of the conformation tensor in viscoelastic fluid models. *Journal of Non-Newtonian Fluid Mechanics* **166** (11), 546–553.

Batchelor, G. 1970*a* The stress system in a suspension of force-free particles. *Journal of fluid mechanics* **41** (3), 545–570.

Batchelor, G. K. 1970*b* The stress system in a suspension of force-free particles. *J. Fluid Mech.* **41**, 545–570.

Batchelor, G. K. 1977 The effect of brownian motion on the bulk stress in a suspension of spherical particles. *J. Fluid Mech.* **83**, 97–117.

Becker, L., McKinley, G. & Stone, H. 1996 Sedimentation of a sphere near a plane wall: weak non-newtonian and inertial effects. *Journal of non-newtonian fluid mechanics* **63** (2-3), 201–233.

Bird, R. B., Armstrong, R. C. & Hassanger, O. 1987 *Dynamics of Polymeric Liquids*. vol. 1. Second edition, Wiley-Interscience.

Bird, R. B. & Wiest, J. M. 1985 Anisotropic effects in dumbbell kinetic theory. *Journal of Rheology* **29** (5), 519–532.

Bobroff, S. & Phillips, R. J. 1998 Nuclear magnetic resonance imaging investigation of sedimentation of concentrated suspensions in non-newtonian fluids. *Journal of Rheology* **42** (6), 1419–1436.

Bonet, J. & Wood, R. D. 1997 *Nonlinear continuum mechanics for finite element analysis*. Cambridge university press.

Bonnoit, C., Lanuza, J., Lindner, A. & Clement, E. 2010 Mesoscopic length scale controls the rheology of dense suspensions. *Physical review letters* **105** (10), 108302.

Bouzid, M., Trulsson, M., Claudin, P., Clément, E. & Andreotti, B. 2013 Nonlocal rheology of granular flows across yield conditions. *Physical review letters* **111** (23), 238301.

Boyer, F., Guazzelli, É. & Pouliquen, O. 2011 Unifying suspension and granular rheology. *Physical Review Letters* **107** (18), 188301.

Brady, J. F. & Bossis, G. 1988 Stokesian dynamics. *Annual review of fluid mechanics* **20** (1), 111–157.

Braun, D. D. & Rosen, M. R. 2013 *Rheology Modifiers Handbook: Practical Use and Applilcation*. Elsevier.

Brenner, H. 1961 The slow motion of a sphere through a viscous fluid towards a plane surface. *Chemical Engineering Science* **16 (3)**, 242–251.

Breugem, W.-P. 2012 A second-order accurate immersed boundary method for fully resolved simulations of particle-laden flows. *Journal of Computational Physics* **231**, 4469–4498.

Breugem, W.-P., Van Dijk, V. & Delfos, R. 2014 Flows through real porous media: x-ray computed tomography, experiments, and numerical simulations. *Journal of Fluids Engineering* **136** (4), 040902.

Bruneau, D., Feuillebois, F., Anthore, R. & Hinch, E. J. 1996 Intrinsic convection in a settling suspension. *Physics of Fluids* **8** (8), 2236–2238.

Bruneau, D., Feuillebois, F., Bławzdziewicz, J. & Anthore, R. 1998 Three-dimensional intrinsic convection in dilute and dense dispersions of settling spheres. *Physics of Fluids* **10** (1), 55–59.

Cassar, C., Nicolas, M. & Pouliquen, O. 2005 Submarine granular flows down inclined planes. *Physics of fluids* **17** (10), 103301.

Chateau, X., Ovarlez, G. & Trung, K. L. 2008 Homogenization approach to the behavior of suspensions of noncolloidal particles in yield stress fluids. *J. Rheol.* **52**, 489–506.

Chen, Y.-L. 2014 Inertia-and deformation-driven migration of a soft particle in confined shear and poiseuille flow. *RSC Advances* **4** (34), 17908–17916.

Chhabra, R. P. 2006 *Bubbles, drops, and particles in non-Newtonian fluids*. CRC press.

Choi, Y.-S., Seo, K.-W. & Lee, S.-J. 2011 Lateral and cross-lateral focusing of spherical particles in a square microchannel. *Lab on a Chip* **11** (3), 460–465.

Clift, R., Grace, J. R. & Weber, M. E. 2005 *Bubbles, drops, and particles*. Courier Corporation.

Climent, E. & Maxey, M. 2003 Numerical simulations of random suspensions at finite reynolds numbers. *International journal of multiphase flow* **29** (4), 579–601.

Costa, P., Boersma, B. J., Westerweel, J. & Breugem, W.-P. 2015 Collision model for fully resolved simulations of flows laden with finite-size particles. *Physical Review E* **92**, 053012.

Costa, P., Picano, F., Brandt, L. & Breugem, W.-P. 2016 Universal scaling laws for dense particle suspensions in turbulent wall-bounded flows. *Physical Review Letters* **117** (13), 134501.

Coupier, G., Kaoui, B., Podgorski, T. & Misbah, C. 2008 Noninertial lateral migration of vesicles in bounded poiseuille flow. *Physics of Fluids* **20** (11), 111702.

Coussot, P., Tocquer, L., Lanos, C. & Ovarlez, G. 2009 Macroscopic vs. local rheology of yield stress fluids. *Journal of Non-Newtonian Fluid Mechanics* **158** (1), 85–90.

Couturier, É., Boyer, F., Pouliquen, O. & Guazzelli, É. 2011 Suspensions in a tilted trough: second normal stress difference. *J . Fluid Mech.* **686**, 26–39.

Cwalina, C. D. & Wagner, N. J. 2014 Material properties of the shear-thickened state in concentrated near hard-sphere colloidal dispersions. *Journal of Rheology* **58** (4), 949–967.

Da Cunha, F. & Hinch, E. J. 1996 Shear-induced dispersion in a dilute suspension of rough spheres. *J. Fluid Mech.* **309**, 211–223.

Dagois-Bohy, S., Hormozi, S., Guazzelli, E. & Pouliquen, O. 2015 Rheology of dense suspensions of non-colloidal spheres in yield-stress fluids. *J. Fluid Mech.* **776**, R2–1–R2–11.

Dai, S.-C., Bertevas, E., Qi, F. & Tanner, R. I. 2013 Viscometric functions for noncolloidal sphere suspensions with newtonian matrices. *Journal of Rheology* **57** (2), 493–510.

Dai, S.-C., Qi, F. & Tanner, R. I. 2014 Viscometric functions of concentrated non-colloidal suspensions of spheres in a viscoelastic matrix. *Journal of Rheology* **58** (1), 183–198.

Daugan, S., Talini, L., Herzhaft, B., Peysson, Y. & Allain, C. 2004 Sedimentation of suspensions in shear-thinning fluids. *Oil & gas science and technology* **59** (1), 71–80.

Davis, R. H. & Acrivos, A. 1985 Sedimentation of noncolloidal particles at low reynolds numbers. *Annual Review of Fluid Mechanics* **17** (1), 91–118.

Dbouk, T., Lemaire, E., Lobry, L. & Moukalled, F. 2013*a* Shear-induced particle

migration: Predictions from experimental evaluation of the particle stress tensor. *Journal of Non-Newtonian Fluid Mechanics* **198**, 78–95.

Dbouk, T., Lobry, L. & Lemaire, E. 2013*b* Normal stresses in concentrated non-brownian suspensions. *J . Fluid Mech.* **715**, 239–272.

De Vita, F., Rosti, M. E., Izbassarov, D., Duffo, L., Tammisola, O., Hormozi, S. & Brandt, L. 2018 Elastoviscoplastic flows in porous media. *Journal of Non-Newtonian Fluid Mechanics* **258**, 10–21.

Deboeuf, A., Gauthier, G., Martin, J., Yurkovetsky, Y. & Morris, J. F. 2009 Particle pressure in a sheared suspension: A bridge from osmosis to granular dilatancy. *Physical review letters* **102** (10), 108301.

DeGiuli, E., Düring, G., Lerner, E. & Wyart, M. 2015 Unified theory of inertial granular flows and non-brownian suspensions. *Physical Review E* **91** (6), 062206.

Di Carlo, D. 2009 Inertial microfluidics. *Lab on a Chip* **9** (21), 3038–3046.

Di Carlo, D., Irimia, D., Tompkins, R. G. & Toner, M. 2007 Continuous inertial focusing, ordering, and separation of particles in microchannels. *Proceedings of the National Academy of Sciences* **104** (48), 18892–18897.

Di Felice, R. 1999 The sedimentation velocity of dilute suspensions of nearly monosized spheres. *International journal of multiphase flow* **25** (4), 559–574.

Doddi, S. K. & Bagchi, P. 2008 Lateral migration of a capsule in a plane poiseuille flow in a channel. *International Journal of Multiphase Flow* **34** (10), 966–986.

Dontsov, E. & Peirce, A. 2014 Slurry flow, gravitational settling, and a proppant transport model for hydraulic fractures .

Einstein, A. 1906 A new determination of the molecular dimensions. *Ann. Phys.* **324, Issue 2**, 289–306.

Einstein, A. 1911 Berichtigung zu meiner arbeit: eine neue bestimmung der moleküldimensionen. *Ann. Phys.* **339** (3), 591–592.

Esteghamatian, A. & Zaki, T. A. 2019 Dilute suspension of neutrally buoyant particles in viscoelastic turbulent channel flow. *Journal of Fluid Mechanics* **875**, 286–320.

Fattal, R. & Kupferman, R. 2004 Constitutive laws for the matrix-logarithm of the conformation tensor. *Journal of Non-Newtonian Fluid Mechanics* **123** (2-3), 281–285.

Fattal, R. & Kupferman, R. 2005 Time-dependent simulation of viscoelastic flows at high weissenberg number using the log-conformation representation. *Journal of Non-Newtonian Fluid Mechanics* **126** (1), 23–37.

Feng, J., Hu, H. H. & Joseph, D. D. 1994 Direct simulation of initial value problems for the motion of solid bodies in a newtonian fluid. part 2. couette and poiseuille flows. *Journal of fluid mechanics* **277**, 271–301.

Firouznia, M., Metzger, B., Ovarlez, G. & Hormozi, S. 2018 The interaction of two spheres in simple shear flows of yield stress fluids. *Journal of Non-Newtonian Fluid Mechanics* **255**, 19–38.

Fornari, W., Ardekani, M. N. & Brandt, L. 2018 Clustering and increased settling speed of oblate particles at finite reynolds number. *Journal of Fluid Mechanics* **848**, 696–721.

Fornari, W., Brandt, L., Chaudhuri, P., Lopez, C. U., Mitra, D. & Picano, F. 2016*a* Rheology of confined non-brownian suspensions. *Phys. rev. lett.* **116** (1), 018301.

Fornari, W., Picano, F. & Brandt, L. 2016*b* Sedimentation of finite-size spheres in quiescent and turbulent environments. *Journal of Fluid Mechanics* **788**, 640–669.

Fornari, W., Zade, S., Brandt, L. & Picano, F. 2019 Settling of finite-size particles in turbulence at different volume fractions. *Acta Mechanica* **230** (2), 413–430.

Garside, J. & Al-Dibouni, M. R. 1977 Velocity-voidage relationships for fluidization and sedimentation in solid-liquid systems. *Industrial & engineering chemistry process design and development* **16** (2), 206–214.

Geigenmüller, U. & Mazur, P. 1988 Sedimentation of homogeneous suspensions in finite vessels. *Journal of statistical physics* **53** (1-2), 137–173.

Giesekus, H. 1982 A simple constitutive equation for polymer fluids based on the concept of deformation-dependent tensorial mobility. *Journal of Non-Newtonian Fluid Mechanics* **11** (1-2), 69–109.

Goyal, N. & Derksen, J. 2012 Direct simulations of spherical particles sedimenting in viscoelastic fluids. *Journal of Non-Newtonian Fluid Mechanics* **183**, 1–13.

Guazzelli, É. & Morris, J. 2011*a* *A Physical Introduction to Suspension Dynamics*. Cambridge Univ Press.

Guazzelli, E. & Morris, J. F. 2011*b* *A physical introduction to suspension dynamics*, , vol. 45. Cambridge University Press.

Guazzelli, É. & Morris, J. F. 2011*c* *A Physical Introduction to Suspension Dynamics*, , vol. 45. Cambridge University Press.

Hadikhani, P., Hashemi, S. M. H., Balestra, G., Zhu, L., Modestino, M. A., Gallaire, F. & Psaltis, D. 2018 Inertial manipulation of bubbles in rectangular microfluidic channels. *Lab on a Chip* **18** (7), 1035–1046.

Henann, D. L. & Kamrin, K. 2014 Continuum modeling of secondary rheology in dense granular materials. *Physical review letters* **113** (17), 178001.

Hill, R. J., Koch, D. L. & Ladd, A. J. 2001 Moderate-reynolds-number flows in ordered and random arrays of spheres. *Journal of Fluid Mechanics* **448**, 243–278.

Ho, B. & Leal, L. 1974 Inertial migration of rigid spheres in two-dimensional unidirectional flows. *Journal of fluid mechanics* **65** (2), 365–400.

Hormozi, S. & Frigaard, I. 2017 Dispersion of solids in fracturing flows of yield stress fluids. *J . Fluid Mech.* **830**, 93–137.

Hsu, J.-P., Shie, C.-F. & Tseng, S. 2005 Sedimentation of a cylindrical particle in a carreau fluid. *Journal of colloid and interface science* **286** (1), 392–399.

Hulsen, M. A., Fattal, R. & Kupferman, R. 2005 Flow of viscoelastic fluids past a cylinder at high weissenberg number: stabilized simulations using matrix logarithms. *Journal of Non-Newtonian Fluid Mechanics* **127** (1), 27–39.

Hur, S. C., Henderson-MacLennan, N. K., McCabe, E. R. & Di Carlo, D. 2011 Deformability-based cell classification and enrichment using inertial microfluidics. *Lab on a Chip* **11** (5), 912–920.

Izbassarov, D. & Muradoglu, M. 2015 A front-tracking method for computational modeling of viscoelastic two-phase flow systems. *Journal of Non-Newtonian Fluid Mechanics* **223**, 122–140.

Izbassarov, D., Rosti, M. E., Ardekani, M. N., Sarabian, M., Hormozi, S., Brandt, L. & Tammisola, O. 2018 Computational modeling of multiphase viscoelastic and elastoviscoplastic flows. *International Journal for Numerical Methods in Fluids* **88** (12), 521–543.

Izdebska, J. & Thomas, S. 2015 *Printing on polymers: fundamentals and applications*. William Andrew.

Janoschek, F. 2013 *Mesoscopic simulation of blood and general suspensions in flow*. Phd thesis at Eindhoven University of Technology.

Jeffrey, D. J. & Acrivos, A. 1976 The rheological properties of suspensions of rigid particles. *AIChE Journal* **22** (3), 417–432.

Johnson, A. A. & Tezduyar, T. E. 1996 Simulation of multiple spheres falling in a liquid-filled tube. *Computer Methods in Applied Mechanics and Engineering* **134** (3), 351–373.

Joseph, D., Liu, Y., Poletto, M. & Feng, J. 1994 Aggregation and dispersion of spheres falling in viscoelastic liquids. *Journal of non-newtonian fluid mechanics* **54**, 45–86.

Kadoch, B., Kolomenskiy, D., Angot, P. & Schneider, K. 2012 A volume penalization method for incompressible flows and scalar advection–diffusion with moving obstacles. *Journal of Computational Physics* **231** (12), 4365–4383.

Kajishima, T., Takiguchi, S., Hamasaki, H. & Miyake, Y. 2001 Turbulence structure of particle-laden flow in a vertical plane channel due to vortex shedding. *JSME International Journal Series B Fluids and Thermal Engineering* **44** (4), 526–535.

Kamrin, K. & Henann, D. L. 2015 Nonlocal modeling of granular flows down inclines. *Soft matter* **11** (1), 179–185.

Kang, K., Lee, S. S., Hyun, K., Lee, S. J. & Kim, J. M. 2013 Dna-based highly tunable particle focuser. *Nature communications* **4**, 2567.

Kaoui, B., Ristow, G., Cantat, I., Misbah, C. & Zimmermann, W. 2008 Lateral migration of a two-dimensional vesicle in unbounded poiseuille flow. *Physical Review E* **77** (2), 021903.

Karimi, A., Yazdi, S. & Ardekani, A. 2013 Hydrodynamic mechanisms of cell and particle trapping in microfluidics. *Biomicrofluidics* **7** (2), 021501.

Karnis, A., Goldsmith, H. & Mason, S. 1966 The flow of suspensions through tubes: V. inertial effects. *The Canadian Journal of Chemical Engineering* **44** (4), 181–193.

Kelessidis, V. C. 2004 An explicit equation for the terminal velocity of solid spheres falling in pseudoplastic liquids. *Chemical engineering science* **59** (21), 4437–4447.

Kempe, T. & Fröhlich, J. 2012 An improved immersed boundary method with direct forcing for the simulation of particle laden flows. *Journal of Computational Physics* **231** (9), 3663–3684.

Kilimnik, A., Mao, W. & Alexeev, A. 2011 Inertial migration of deformable capsules in channel flow. *Physics of fluids* **23** (12), 123302.

Kim, B., Chang, C. B., Park, S. G. & Sung, H. J. 2015 Inertial migration of a 3d elastic capsule in a plane poiseuille flow. *International Journal of Heat and Fluid Flow* **54**, 87–96.

Kim, J. & Moin, P. 1985 Application of a fractional-step method to incompressible navier-stokes equations. *Journal of computational physics* **59** (2), 308–323.

Konijn, B., Sanderink, O. & Kruyt, N. 2014 Experimental study of the viscosity of suspensions: Effect of solid fraction, particle size and suspending liquid. *Powder Technology* **266**, 61–69.

Krieger, I. M. & Dougherty, T. J. 1959 A mechanism for non-newtonian flow in suspensions of rigid spheres. *Trans. Soc. of Rheo.* **3** (1), 137–152.

Krüger, T., Kaoui, B. & Harting, J. 2014 Interplay of inertia and deformability on rheological properties of a suspension of capsules. *Journal of Fluid Mechanics* **751**, 725–745.

Kulkarni, P. M. & Morris, J. F. 2008*a* Suspension properties at finite Reynolds number from simulated shear flow. *Phys. Fluids* **20**, 040602.

Kulkarni, P. M. & Morris, J. F. 2008*b* Suspension properties at finite Reynolds number from simulated shear flow. *Phys. Fluids* **20**, 040602.

Kulkarni, P. M. & Morris, J. F. 2008*c* Suspension properties at finite reynolds number from simulated shear flow. *Phys. Fluids* **20**, 040602.

Ladd, A. J. 1993 Dynamical simulations of sedimenting spheres. *Physics of Fluids A: Fluid Dynamics (1989-1993)* **5** (2), 299–310.

Ladd, A. J. 1994*a* Numerical simulations of particulate suspensions via a discretized boltzmann equation. part 1. theoretical foundation. *Journal of Fluid Mechanics* **271**, 285–309.

Ladd, A. J. 1994*b* Numerical simulations of particulate suspensions via a discretized boltzmann equation. part 2. numerical results. *Journal of Fluid Mechanics* **271**, 311–339.

Lambert, R., Picano, F., Breugem, W. P. & Brandt, L. 2013 Active suspensions in thin films: nutrient uptake and swimmer motion. *J. Fluid Mech.* **733**, 528–557.

Larson, R. G. 1988 *Constitutive equations for polymer melts and solutions*. Elsevier.

Larson, R. G. 1999 *The structure and rheology of complex fluids*, , vol. 150. Oxford university press New York.

Lashgari, I., Ardekani, M. N., Banerjee, I., Russom, A. & Brandt, L. 2017 Inertial migration of spherical and oblate particles in straight ducts. *Journal of Fluid Mechanics* **819**, 540–561.

Lashgari, I., Picano, F., Breugem, W.-P. & Brandt, L. 2014 Laminar, turbulent and inertial shear-thickening regimes in channel flow of neutrally buoyant particle suspensions. *Phys. Rev. Lett.* **113**, 254502.

Lashgari, I., Picano, F., Breugem, W. P. & Brandt, L. 2016 Channel flow of rigid sphere suspensions:particle dynamics in the inertial regime. *International Journal of Multiphase Flow* **78**, 12–24.

Lázaro, G. R., Hernández-Machado, A. & Pagonabarraga, I. 2014 Rheology of red blood cells under flow in highly confined microchannels. ii. effect of focusing and confinement. *Soft matter* **10** (37), 7207–7217.

Leshansky, A. M., Bransky, A., Korin, N. & Dinnar, U. 2007 Tunable nonlinear viscoelastic "focusing" in a microfluidic device. *Physical review letters* **98** (23), 234501.

Li, G., McKinley, G. H. & Ardekani, A. M. 2015 Dynamics of particle migration in channel flow of viscoelastic fluids. *Journal of Fluid Mechanics* **785**, 486–505.

Liard, M., Martys, N. S., George, W. L., Lootens, D. & Hebraud, P. 2014 Scaling laws for the flow of generalized newtonian suspensions. *J. Rheol.:* **58**, 1993–2015.

Lim, H., Nam, J. & Shin, S. 2014 Lateral migration of particles suspended in viscoelastic fluids in a microchannel flow. *Microfluidics and nanofluidics* **17** (4), 683.

Linares-Guerrero, E., Hunt, M. L. & Zenit, R. 2017 Effects of inertia and turbulence on rheological measurements of neutrally buoyant suspensions. *J . Fluid Mech.* **811**, 525–543.

Liu, X.-D., Osher, S. & Chan, T. 1994 Weighted essentially non-oscillatory schemes. *J. Comput. Phys.* **115**, 200–213.

Lomholt, S. & Maxey, M. 2003 Force-coupling method for particulate two-phase flow: Stokes flow. *Journal of Computational Physics* **184** (2), 381–405.

Lu, X., Liu, C., Hu, G. & Xuan, X. 2017 Particle manipulations in non-newtonian microfluidics: A review. *Journal of colloid and interface science* **500**, 182–201.

Luo, K., Wang, Z., Fan, J. & Cen, K. 2007 Full-scale solutions to particle-laden flows: Multidirect forcing and immersed boundary method. *Physical Review E* **76** (6), 066709.

Lyon, M., Mead, D., Elliott, R. & Leal, L. 2001 Structure formation in moderately concentrated viscoelastic suspensions in simple shear flow. *Journal of Rheology* **45** (4), 881–890.

Mach, A. J. & Di Carlo, D. 2010 Continuous scalable blood filtration device using inertial microfluidics. *Biotechnology and bioengineering* **107** (2), 302–311.

Madraki, Y., Hormozi, S., Ovarlez, G., Guazzelli, E. & Pouliquen, O. 2017 Enhancing shear thickening. *Physical Review Fluids* **2** (3), 033301.

Mahaut, F., Chateau, X., Coussot, P. & Ovarlez, G. 2008 Yield stress and elastic modulus of suspensions of noncolloidal particles in yield stress fluids. *Journal of Rheology* **52** (1), 287–313.

Malhotra, S. & Sharma, M. M. 2012 Settling of spherical particles in unbounded and confined surfactant-based shear thinning viscoelastic fluids: An experimental study. *Chemical engineering science* **84**, 646–655.

Maron, S. H. & Pierce, P. E. 1956 Application of ree-eyring generalized flow theory to suspensions of spherical particles. *J. Colloid Sci.* **11**, 80–95.

Martel, J. M. & Toner, M. 2014 Inertial focusing in microfluidics. *Annual review of biomedical engineering* **16**, 371–396.

Matas, J.-P., Morris, J. F. & Guazzelli, É. 2004 Inertial migration of rigid spherical particles in poiseuille flow. *Journal of Fluid Mechanics* **515**, 171–195.

Maxey, M. 2017 Simulation methods for particulate flows and concentrated suspensions. *Annual Review of Fluid Mechanics* **49**, 171–193.

Mendoza, C. I. & Santamaria-Holek, I. 2009 The rheology of hard sphere suspensions at arbitrary volume fractions: An improved differential viscosity model. *J. Chem. Phys.* **130**, 044904.

Mewis, J. & Wagner, N. J. 2012 *Colloidal suspension rheology*. Cambridge University Press.

Mezger, T. G. 2015 *Applied rheology: with Joe flow on rheology road*. Anton Paar.

Michele, J., Pätzold, R. & Donis, R. 1977 Alignment and aggregation effects in suspensions of spheres in non-newtonian media. *Rheologica Acta* **16** (3), 317–321.

Min, T., Yoo, J. Y. & Choi, H. 2001 Effect of spatial discretization schemes on numerical solutions of viscoelastic fluid flows. *Journal of non-newtonian fluid mechanics* **100** (1-3), 27–47.

Mittal, R. & Iaccarino, G. 2005 Immersed boundary methods. *Annual Review of Fluid Mechanics* **37**, 239–261.

Mokbel, M., Mokbel, D., Mietke, A., Traber, N., Girardo, S., Otto, O.,

Guck, J. & Aland, S. 2017 Numerical simulation of real-time deformability cytometry to extract cell mechanical properties. *ACS Biomaterials Science & Engineering* **3** (11), 2962–2973.

Morrison, F. 2001 *Understanding Rheology*. 1st ed., Oxford University Press, Inc.,Madison Avenue, New York.

Nicolai, H., Herzhaft, B., Hinch, E., Oger, L. & Guazzelli, E. 1995 Particle velocity fluctuations and hydrodynamic self-diffusion of sedimenting non-brownian spheres. *Physics of Fluids* **7** (1), 12–23.

Nouar, C., Bottaro, A. & Brancher, J. P. 2007 Delaying transition to turbulence in channel flow: revisiting the stability of shear-thinning fluids. *J . Fluid Mech.* **592**, 177–194.

Oldroyd, J. G. 1950 On the formulation of rheological equations of state. *Proceedings of the Royal Society of London. Series A. Mathematical and Physical Sciences* **200** (1063), 523–541.

Orlandi, P. & Leonardi, S. 2008 Direct numerical simulation of three-dimensional turbulent rough channels: parameterization and flow physics. *Journal of Fluid Mechanics* **606**, 399–415.

Ovarlez, G., Bertrand, F., Coussot, P. & Chateau, X. 2012 Shear-induced sedimentation in yield stress fluids. *Journal of Non-Newtonian Fluid Mechanics* **177**, 19–28.

Ovarlez, G., Bertrand, F. & Rodts, S. 2006 Local determination of the constitutive law of a dense suspension of noncolloidal particles through magnetic resonance imaging. *Journal of Rheology* **50** (3), 259–292.

Ovarlez, G., Mahaut, F., Deboeufg, S., Lenoir, N., Hormozi, S. & Chateau, X. 2015 Flows of suspensions of particles in yield stress fluids. *J. Rheol.:* **59**, 1449–1486.

Pamme, N. 2007 Continuous flow separations in microfluidic devices. *Lab on a Chip* **7** (12), 1644–1659.

Peskin, C. 1972 Flow patterns around heart valves: a numerical method. *Journal of computational physics* **10** (2), 252–271.

Peysson, Y. & Guazzelli, E. 1998 An experimental investigation of the intrinsic convection in a sedimenting suspension. *Physics of Fluids* **10** (1), 44–54.

Phan-Thien, N. & Mai-Duy, N. 2017 *Understanding viscoelasticity: an introduction to rheology*. Springer.

Picano, F., Breugem, W.-P. & Brandt, L. 2015 Turbulent channel flow of dense suspensions of neutrally buoyant spheres. *J. Fluid Mech.* **764**, 463–487.

Picano, F., Breugem, W.-P., Mitra, D. & Brandt, L. 2013 Shear thickening in non-Brownian suspensions: An excluded volume effect. *Phys. Rev. Lett.* **111** (9), 098302.

Pignatel, F., Nicolas, M. & Guazzelli, E. 2011 A falling cloud of particles at a small but finite reynolds number. *Journal of Fluid Mechanics* **671**, 34–51.

Pimenta, F. & Alves, M. 2017 Stabilization of an open-source finite-volume solver for viscoelastic fluid flows. *Journal of Non-Newtonian Fluid Mechanics* **239**, 85–104.

Pope, S. 2000 *Turbulent flows*. Cambridge University Press.

Poslinski, A. J., Ryan, M. E., Gupta, R. K., Seshadri, S. G. & Frechette,

F. J. 1988 Rheological behavior of filled polymeric systems i. yield stress and shear-thinning effects. *Journal of Rheology* **32** (7), 703–735.

Pouliquen, O. & Forterre, Y. 2009 A non-local rheology for dense granular flows. *Philosophical Transactions of the Royal Society of London A: Mathematical, Physical and Engineering Sciences* **367** (1909), 5091–5107.

Prosperetti, A. 2015 Life and death by boundary conditions. *J. Fluid Mech.* **768**, 1–4.

Putz, A., Burghelea, T., Frigaard, I. & Martinez, D. 2008 Settling of an isolated spherical particle in a yield stress shear thinning fluid. *Physics of Fluids* **20** (3), 033102.

Quemada, D. 1977 Rheology of concentrated disperse systems and minimum energy dissipation principle. i. viscosity-concentration relationship. *Rheol. Acta* **16**, 82–94.

Quintard, M. & Whitaker, S. 1994 Transport in ordered and disordered porous media ii: Generalized volume averaging. *Transport in porous media* **14** (2), 179–206.

Raffiee, A. H., Dabiri, S. & Ardekani, A. M. 2017 Elasto-inertial migration of deformable capsules in a microchannel. *Biomicrofluidics* **11** (6), 064113.

Rajitha, P., Chhabra, R., Sabiri, N. & Comiti, J. 2006 Drag on non-spherical particles in power law non-newtonian media. *International Journal of Mineral Processing* **78** (2), 110–121.

Revstedt, J. 2004 A virtual boundary method with improved computational efficiency using a multi-grid method. *International journal for numerical methods in fluids* **45** (7), 775–795.

Revstedt, J. 2013 Interaction between an incompressible flow and elastic cantilevers of circular cross-section. *International Journal of Heat and Fluid Flow* **43**, 244–250.

Revstedt, J. & Fuchs, L. 2001 Handling complex boundaries on a cartesian grid using surface singularities. *International journal for numerical methods in fluids* **35** (2), 125–150.

Reynolds, P. & Jones, T. 1989 An experimental study of the settling velocities of single particles in non-newtonian fluids. *International Journal of Mineral Processing* **25** (1-2), 47–77.

Richardson, J. & Zaki, W. 1954 The sedimentation of a suspension of uniform spheres under conditions of viscous flow. *Chemical Engineering Science* **3** (2), 65–73.

Risso, F., Collé-Paillot, F. & Zagzoule, M. 2006 Experimental investigation of a bioartificial capsule flowing in a narrow tube. *Journal of fluid mechanics* **547**, 149–173.

Roma, A., Peskin, C. & Berger, M. 1999 An adaptive version of the immersed boundary method. *Journal of computational physics* **153** (2), 509–534.

Rosti, M. E. & Brandt, L. 2017*a* Numerical simulation of turbulent channel flow over a viscous hyper-elastic wall. *Journal of Fluid Mechanics* **830**, 708–735.

Rosti, M. E. & Brandt, L. 2017*b* Numerical simulation of turbulent channel flow over a viscous hyper-elastic wall. *Journal of Fluid Mechanics* **830**, 708–735.

Rosti, M. E. & Brandt, L. 2018 Suspensions of deformable particles in a Couette flow. *Journal of Non-Newtonian Fluid Mechanics* **262** (C), 3–11.

Rosti, M. E., Brandt, L. & Mitra, D. 2018 Rheology of suspensions of viscoelastic spheres: Deformability as an effective volume fraction. *Physical Review Fluids* **3** (1), 012301(R).

Rosti, M. E., De Vita, F. & Brandt, L. 2019*a* Numerical simulations of emulsions in shear flows. *Acta Mechanica* **230** (2), 667–682.

Rosti, M. E., Picano, F. & Brandt, L. 2019*b* Numerical approaches to complex fluids. In *Flowing Matter*, pp. 1–34. Springer.

Salac, D. & Miksis, M. J. 2012 Reynolds number effects on lipid vesicles. *Journal of Fluid Mechanics* **711**, 122–146.

Saramito, P. 2016 *Complex fluids*. Springer.

Schaaf, C. & Stark, H. 2017 Inertial migration and axial control of deformable capsules. *Soft matter* **13** (19), 3544–3555.

Schleiniger, G. & Weinacht, R. J. 1991 A remark on the giesekus viscoelastic fluid. *Journal of Rheology* **35** (6), 1157–1170.

Schonberg, J. A. & Hinch, E. 1989 Inertial migration of a sphere in poiseuille flow. *Journal of Fluid Mechanics* **203**, 517–524.

Schumann, U. & Sweet, R. A. 1988 Fast fourier transforms for direct solution of poisson's equation with staggered boundary conditions. *Journal of Computational Physics* **75** (1), 123–137.

Scirocco, R., Vermant, J. & Mewis, J. 2004 Effect of the viscoelasticity of the suspending fluid on structure formation in suspensions. *Journal of Non-Newtonian Fluid Mechanics* **117** (2-3), 183–192.

Scirocco, R., Vermant, J. & Mewis, J. 2005 Shear thickening in filled boger fluids. *Journal of Rheology* **49** (2), 551–567.

Segre, G. & Silberberg, A. 1961 Radial particle displacements in poiseuille flow of suspensions. *Nature* **189** (4760), 209.

Shah, S. N., El Fadili, Y. & Chhabra, R. 2007 New model for single spherical particle settling velocity in power law (visco-inelastic) fluids. *International journal of multiphase flow* **33** (1), 51–66.

Shahmardi, A., Zade, S., Ardekani, M. N., Poole, R. J., Lundell, F., Rosti, M. E. & Brandt, L. 2019*a* Turbulent duct flow with polymers. *Journal of Fluid Mechanics* **859**, 1057–1083.

Shahmardi, A., Zade, S., Ardekani, M. N., Poole, R. J., Lundell, F., Rosti, M. E. & Brandt, L. 2019*b* Turbulent duct flow with polymers. *Journal of Fluid Mechanics* **859**, 1057–1083.

Shewan, H. & Stokes, J. 2015 Analytically predicting the viscosity of hard sphere suspensions from the particle size distribution. *J. Non-Newt. Fluid Mech.* **222**, 72–81.

Shin, S. J. & Sung, H. J. 2011 Inertial migration of an elastic capsule in a poiseuille flow. *Physical Review E* **83** (4), 046321.

Shu, C.-W. 2009 High order weighted essentially nonoscillatory schemes for convection dominated problems. *SIAM review* **51** (1), 82–126.

Sierakowski, A. & Prosperetti, A. 2016 Resolved-particle simulation by the physalis method: Enhancements and new capabilities. *Journal of Computational Physics* **309**, 164–184.

Sierou, A. & Brady, J. F. 2002 Rheology and microstructure in concentrated noncolloidal suspensions. *Journal of Rheology* **46** (5), 1031–1056.

Sierou, A. & Brady, J. F. 2004 Shear-induced self-diffusion in non-colloidal suspensions. *J. Fluid Mech.* **506**, 285–314.

Singh, A. & Nott, P. 2003 Experimental measurements of the normal stresses in sheared stokesian suspensions. *J. Fluid Mech.* **490**, 293–320.

Snijkers, F., ĎAvino, G., Maffettone, P., Greco, F., Hulsen, M. & Vermant, J. 2011 Effect of viscoelasticity on the rotation of a sphere in shear flow. *Journal of Non-Newtonian Fluid Mechanics* **166** (7-8), 363–372.

Spalart, P., Moser, R. & Rogers, M. 1991 Spectral methods for the navier-stokes equations with one infinite and two periodic directions. *Journal of Computational Physics* **96** (2), 297–324.

Stickel, J. & Powell, R. 2005 Fluid mechanics and rheology of dense suspensions. *Annu. Rev. Fluid Mech.* **37**, 129–149.

Stoecklein, D. & Di Carlo, D. 2018 Nonlinear microfluidics. *Analytical chemistry* **91** (1), 296–314.

Sugiyama, K., Ii, S., Takeuchi, S., Takagi, S. & Matsumoto, Y. 2011 A full eulerian finite difference approach for solving fluid–structure coupling problems. *Journal of Computational Physics* **230** (3), 596–627.

Takeuchi, S., Yuki, Y., Ueyama, A. & Kajishima, T. 2010 A conservative momentum-exchange algorithm for interaction problem between fluid and deformable particles. *International Journal for Numerical Methods in Fluids* **64** (10-12), 1084–1101.

Ten Cate, A., Derksen, J. J., Portela, L. M. & Van Den Akker, H. E. 2004 Fully resolved simulations of colliding monodisperse spheres in forced isotropic turbulence. *Journal of Fluid Mechanics* **519**, 233–271.

Tirtaatmadja, V. & Sridhar, T. 1995 Comparison of constitutive equations for polymer solutions in uniaxial extension. *Journal of Rheology* **39** (6), 1133–1160.

Trulsson, M., Andreotti, B. & Claudin, P. 2012 Transition from the viscous to inertial regime in dense suspensions. *Physical review letters* **109** (11), 118305.

Tryggvason, G., Sussman, M. & Hussaini, M. 2007 Immersed boundary methods for fluid interfaces. *Computational methods for multiphase flow* **3**.

Turton, R. & Clark, N. 1987 An explicit relationship to predict spherical particle terminal velocity. *Powder Technology* **53** (2), 127–129.

Uhlmann, M. 2005 An immersed boundary method with direct forcing for simulation of particulate flow. *J. Comput. Phys.* **209**, 448–476.

Uhlmann, M. & Doychev, T. 2014 Sedimentation of a dilute suspension of rigid spheres at intermediate galileo numbers: the effect of clustering upon the particle motion. *Journal of Fluid Mechanics* **752**, 310–348.

Unverdi, S. & Tryggvason, G. 1992 A front-tracking method for viscous, incompressible, multi-fluid flows. *Journal of computational physics* **100** (1), 25–37.

Verma, M. & Kumaran, V. 2013 A multifold reduction in the transition reynolds number, and ultra-fast mixing, in a micro-channel due to a dynamical instability induced by a soft wall. *Journal of Fluid Mechanics* **727**, 407–455.

Villone, M. M., Greco, F., Hulsen, M. A. & Maffettone, P. L. 2016 Numerical simulations of deformable particle lateral migration in tube flow of newtonian and viscoelastic media. *Journal of Non-Newtonian Fluid Mechanics* **234**, 105–113.

Vitkova, V., Mader, M. & Podgorski, T. 2004 Deformation of vesicles flowing through capillaries. *EPL (Europhysics Letters)* **68** (3), 398.

Vu, T., Ovarlez, G. & Chateau, X. 2010 Macroscopic behavior of bidisperse suspensions of noncolloidal particles in yield stress fluids. *Journal of Rheology* **54** (4), 815–833.

Wang, Z., Sui, Y., Salsac, A.-V., Barthès-Biesel, D. & Wang, W. 2016 Motion of a spherical capsule in branched tube flow with finite inertia. *Journal of Fluid Mechanics* **806**, 603–626.

Wesseling, P. 2009 *Principles of computational fluid dynamics*, , vol. 29. Springer Science & Business Media.

Xuan, X., Zhu, J. & Church, C. 2010 Particle focusing in microfluidic devices. *Microfluidics and nanofluidics* **9** (1), 1–16.

Yang, B. H., Wang, J., Joseph, D. D., Hu, H. H., Pan, T.-W. & Glowinski, R. 2005 Migration of a sphere in tube flow. *Journal of Fluid Mechanics* **540**, 109–131.

Yang, M., Krishnan, S. & Shaqfeh, E. S. 2016 Numerical simulations of the rheology of suspensions of rigid spheres at low volume fraction in a viscoelastic fluid under shear. *Journal of Non-Newtonian Fluid Mechanics* **233**, 181–197.

Yang, M. & Shaqfeh, E. S. G. 2018*a* Mechanism of shear thickening in suspensions of rigid spheres in Boger fluids. Part I: Dilute suspensions. *Journal of Rheology* **62** (6), 1363–1377.

Yang, M. & Shaqfeh, E. S. G. 2018*b* Mechanism of shear thickening in suspensions of rigid spheres in Boger fluids. Part II: Suspensions at finite concentration. *Journal of Rheology* **62** (6), 1379–1396.

Yang, S., Kim, J. Y., Lee, S. J., Lee, S. S. & Kim, J. M. 2011 Sheathless elasto-inertial particle focusing and continuous separation in a straight rectangular microchannel. *Lab on a Chip* **11** (2), 266–273.

Yeo, K. & Maxey, M. R. 2010*a* Dynamics of concentrated suspensions of non-colloidal particles in couette flow. *J . Fluid Mech.* **649**, 205–231.

Yeo, K. & Maxey, M. R. 2010*b* Dynamics of concentrated suspensions of non-colloidal particles in couette flow. *Journal of Fluid Mechanics* **649**, 205–231.

Yeo, K. & Maxey, M. R. 2011 Numerical simulations of concentrated suspensions of monodisperse particles in a Poiseuille flow. *J. Fluid Mech.* **682**, 491–518.

Yeo, K. & Maxey, M. R. 2013 Dynamics and rheology of concentrated, finite-reynolds-number suspensions in a homogeneous shear flow. *Phys. Fluids* **25** (5), 053303.

Yin, X. & Koch, D. L. 2007 Hindered settling velocity and microstructure in suspensions of solid spheres with moderate reynolds numbers. *Physics of Fluids (1994-present)* **19** (9), 093302.

Yu, Z., Phan-Thien, N., Fan, Y. & Tanner, R. I. 2002 Viscoelastic mobility problem of a system of particles. *Journal of non-newtonian fluid mechanics* **104** (2-3), 87–124.

Yu, Z., Wachs, A. & Peysson, Y. 2006*a* Numerical simulation of particle sedimentation in shear-thinning fluids with a fictitious domain method. *Journal of Non-Newtonian Fluid Mechanics* **136** (2-3), 126–139.

Yu, Z., Wachs, A. & Peysson, Y. 2006*b* Numerical simulation of particle sedimentation in shear-thinning fluids with a fictitious domain method. *Journal of non-newtonian fluid mechanics* **136** (2), 126–139.

Yurkovetsky, Y. & Morris, J. F. 2008 Particle pressure in sheared brownian suspensions. *Journal of rheology* **52** (1), 141–164.

Zarraga, I., Hill, D. & Leighton, D. 2000 The characterization of the total stress of concentrated suspensions of noncolloidal spheres in newtonian fluids. *J. Rheol.* **44**, 185–220.

Zarraga, I. E., Hill, D. A. & Leighton Jr, D. T. 2001 Normal stresses and free surface deformation in concentrated suspensions of noncolloidal spheres in a viscoelastic fluid. *Journal of Rheology* **45** (5), 1065–1084.

Zhang, G.-D., Li, M.-Z., Xue, J.-Q., Wang, L. & Tian, J.-L. 2016 Wall-retardation effects on particles settling through non-newtonian fluids in parallel plates. *Chemical Papers* **70** (10), 1389–1398.

Zhang, Q. & Prosperetti, A. 2010 Physics-based analysis of the hydrodynamic stress in a fluid-particle system. *Phys. Fluid* **22**, 033306.

Zhang, Z. & Prosperetti, A. 2005 A second-order method for three-dimensional particle simulation. *Journal of Computational Physics* **210** (1), 292–324.

Zhu, L., Lauga, E. & Brandt, L. 2012 Self-propulsion in viscoelastic fluids: Pushers vs. pullers. *Physics of fluids* **24** (5), 051902.

Zhu, L. & Peskin, C. S. 2003 Interaction of two flapping filaments in a flowing soap film. *Physics of fluids* **15** (7), 1954–1960.

Zhu, L., Rorai, C., Mitra, D. & Brandt, L. 2014 A microfluidic device to sort capsules by deformability: a numerical study. *Soft Matter* **10** (39), 7705–7711.